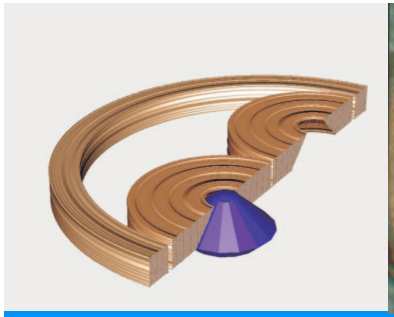


Applications of NRIXS and NFS Techniques at High Pressures

by Viktor V. Struzhkin

Carnegie Institution of Washington
Geophysical Laboratory

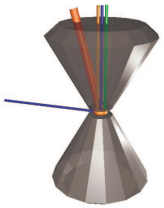

Collaboration

J. F. Lin, H. K. Mao, W. Mao, J. Xu, J. Hu, J. Shu, R. J. Hemley	*GL, CIW Washington DC*
W. Sturhahn, J. Zhao E. E. Alp	*APS, ANL, Argonne, IL*
M. Y. Hu, M. Schwoerer-Böning, D. Häusermann, D. Errandonnea	*HPCAT, ANL, Argonne, IL*
L. Vocadlo, D. Alfè, G.D. Price, M.J. Gillan	*University College London, UK*
M. I. Eremets	*Max-Planck Institute, Mainz, Germany*
E. Huang	*Institute for Earth Sciences, Taiwan*

Support

DOE (DE-FG02-02ER459555)
NSF
W. M. Keck Foundation

Outline

- Electronic correlations in simple oxides
- Phonon and magnon excitations in iron oxide - magnetoelastic coupling
- P-T magnetic phase diagram of $Fe_{0.94}O$
- Insulator-metal transition in $Fe_{0.94}O$
- Elastic properties of iron from NRIXS studies

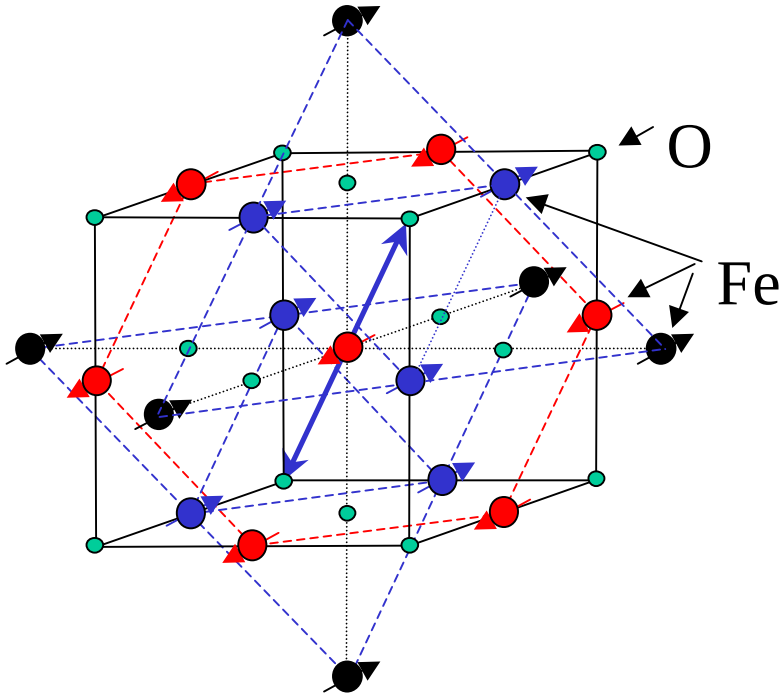
O
Fe

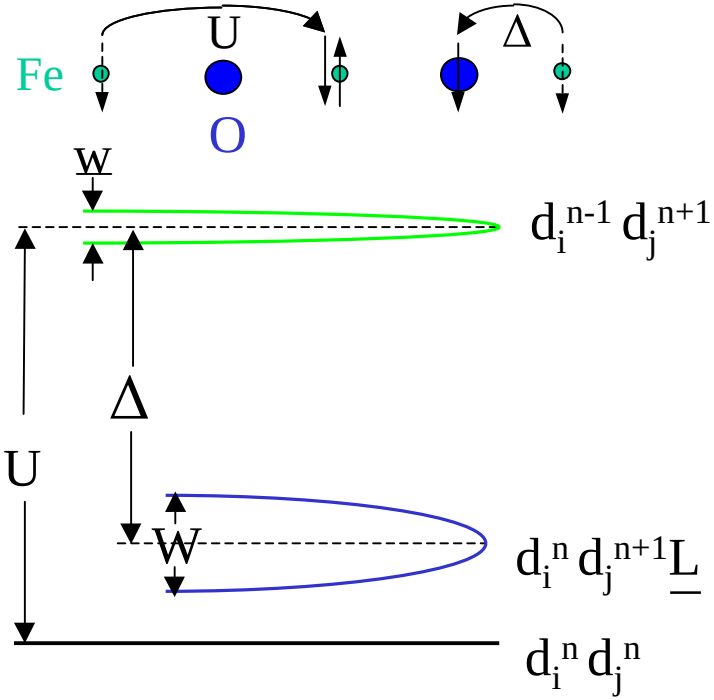
Fe
U
Δ
O
W
$d_i^{n-1} d_j^{n+1}$
Δ
U
W
$d_i^{n} d_j^{n+1}\underline{L}$
$d_i^{n} d_j^{n}$

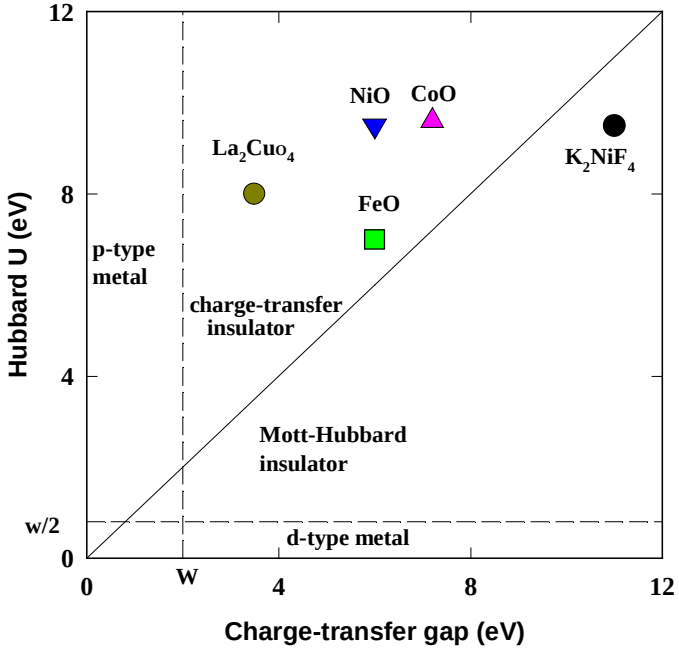
12
8
4
w/2
0
Hubbard U (eV)
NiO
CoO
La_2Cuo_4
K_2NiF_4
FeO
p-type
metal
charge-transfer
insulator
Mott-Hubbard
insulator
d-type metal
0
W
4
8
12
Charge-transfer gap (eV)

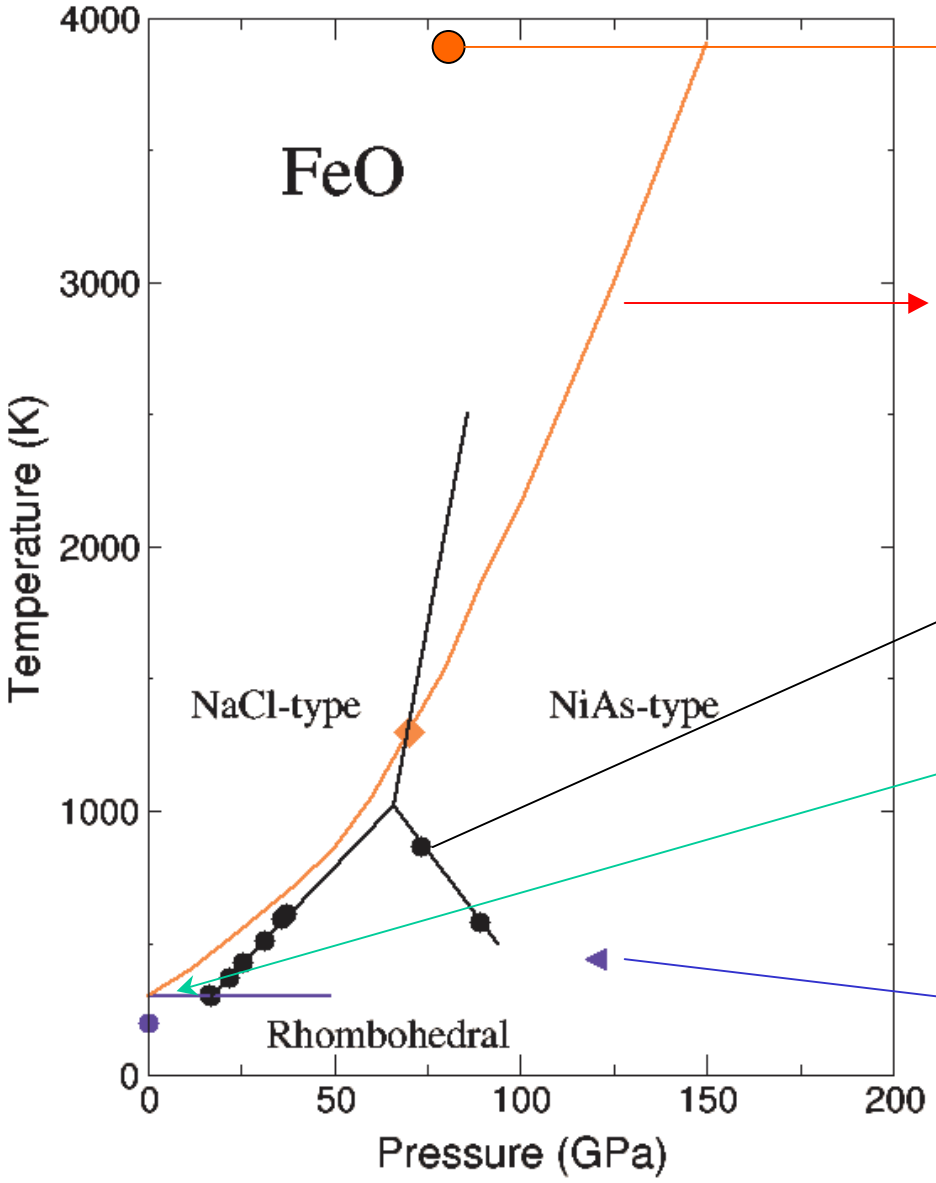

Metallic FeO under laser heating

E. Knittle, R. Jeanloz (1991)

Shock-wave experiment, Hugoniot temperature and phase transition at 70 GPa

R. Jeanloz, T. J. Ahrens (1980)

In situ X-ray diffraction

Y. Fei, H. K. Mao (1994)

Soft C_{44}

I. Jackson et al. (1990)

A. K. Singh et al. (1998)

Mössbauer (magnetic transition)

M. Pasternak et al. (1998)

Magnetic collapse in transition metal oxides

Cohen, Mazin, Isaak, Science 1997

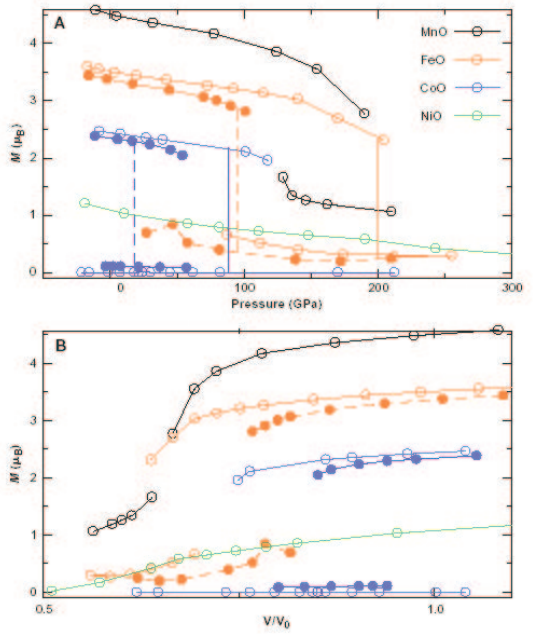

R. E. Cohen et al., MRS Symp proc. 1998

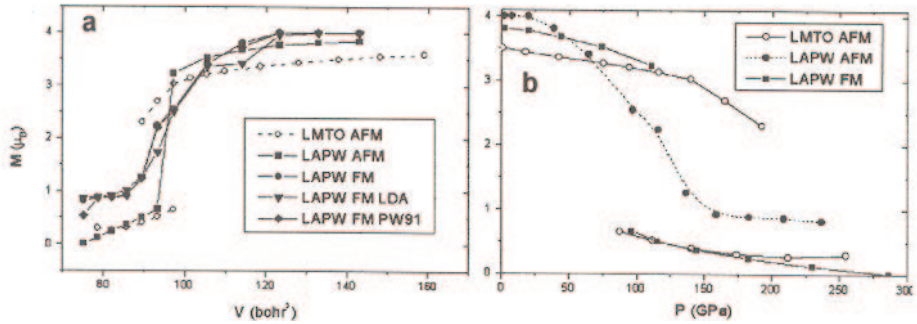

High-spin to low-spin transition

I. Jackson and A. E. Ringwood (1981)

$$\Delta G = \Delta E - P\Delta V + T\Delta S$$

$$\Delta E = Nn\{\pi - \Delta(r)\},\ \ \Delta \sim \Delta_0 (r_0/r)^5$$

For cubic (B1) FeO: P_{tr}=50 GPa

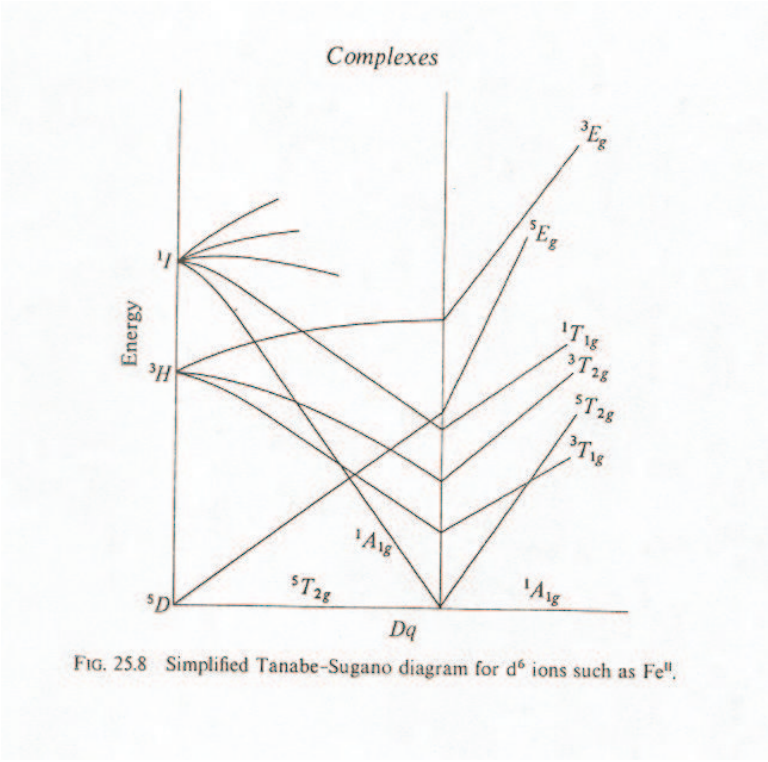

FIG. 25.8 Simplified Tanabe-Sugano diagram for d^6 ions such as Fe^{II}.

Comparison of Mössbauer and X-ray emission results: FeO

M. P. Pasternak et al . Phys. Rev. Lett.(1997)

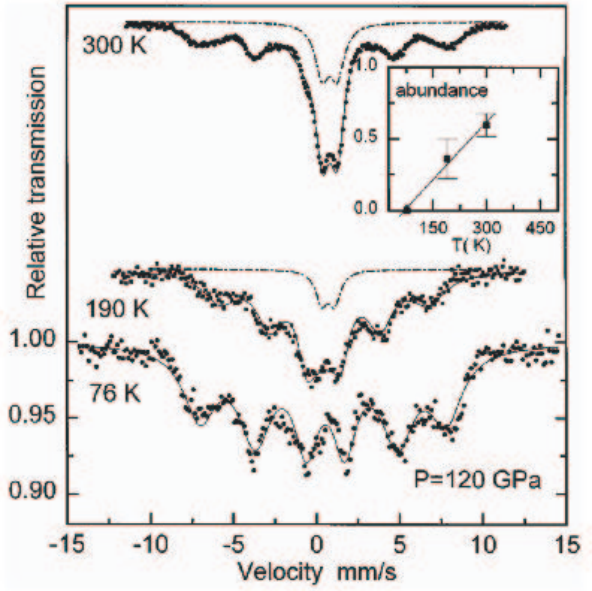

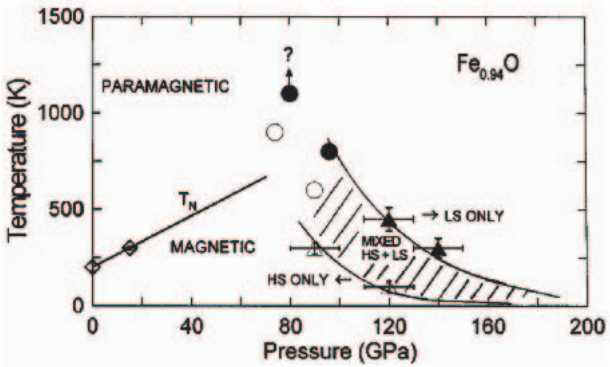

J. Badro et al. Phys. Rev. Lett. (1999)

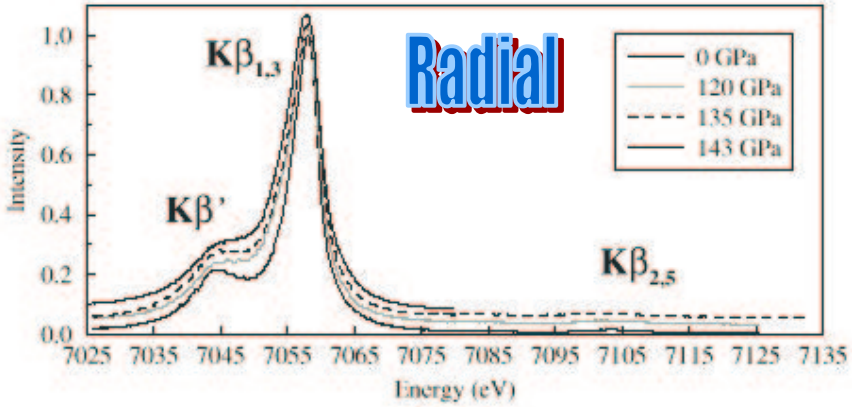

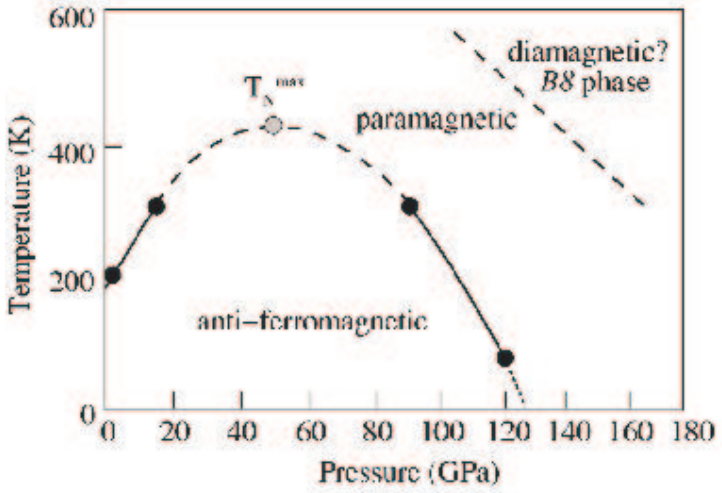

Nuclear inelastic scattering set-up
(W. Sturhahn, E. Alp, M. Hu)

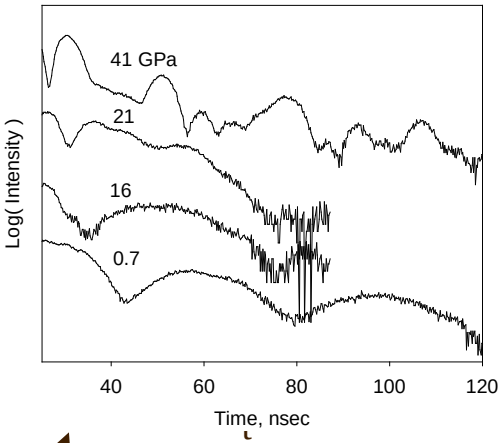

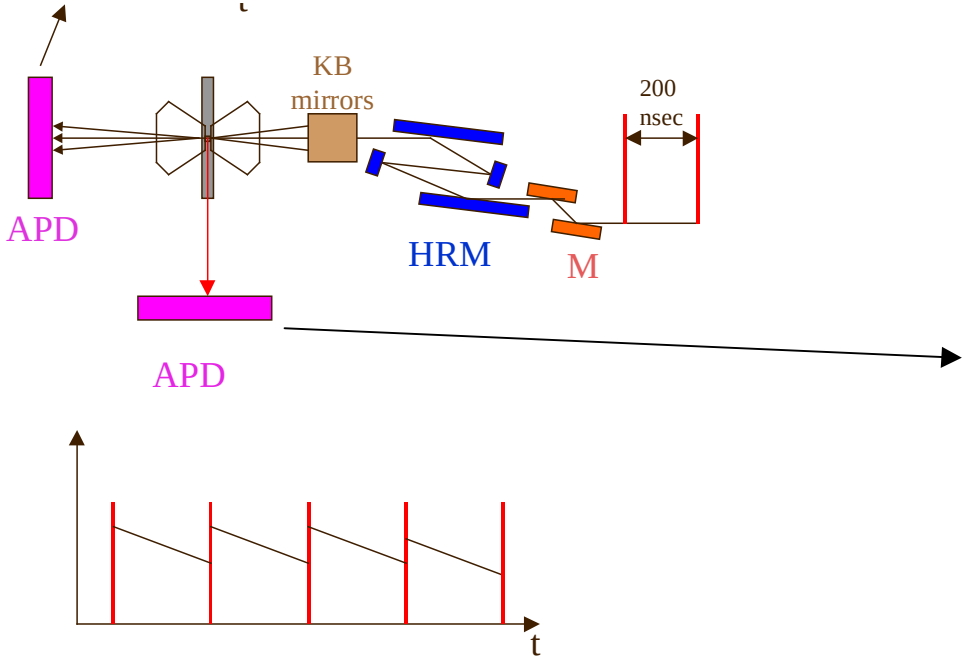

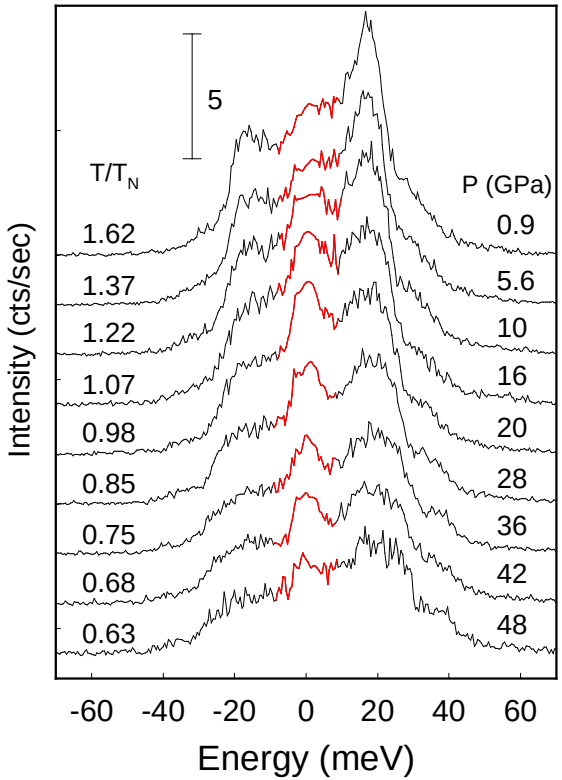

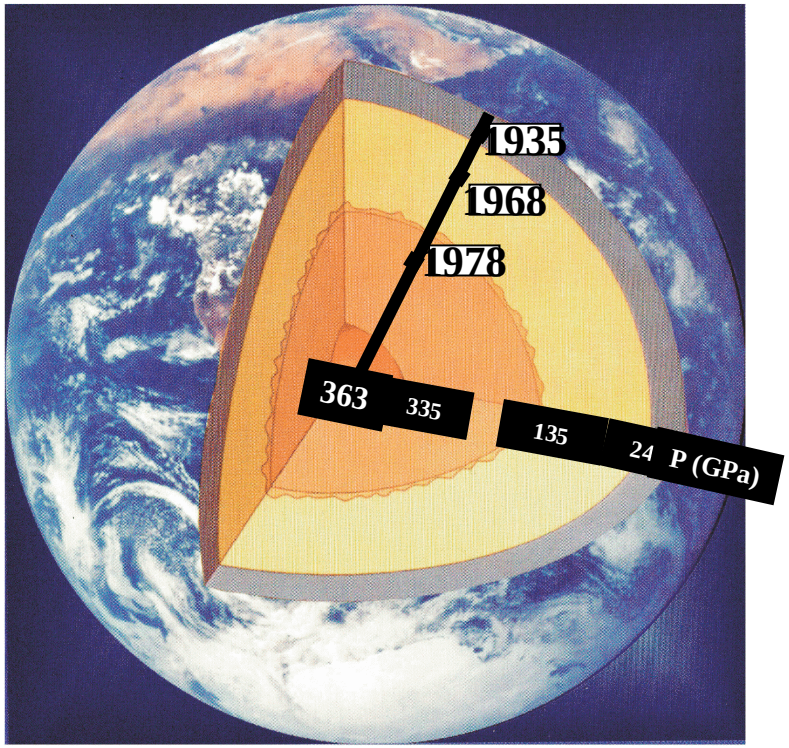

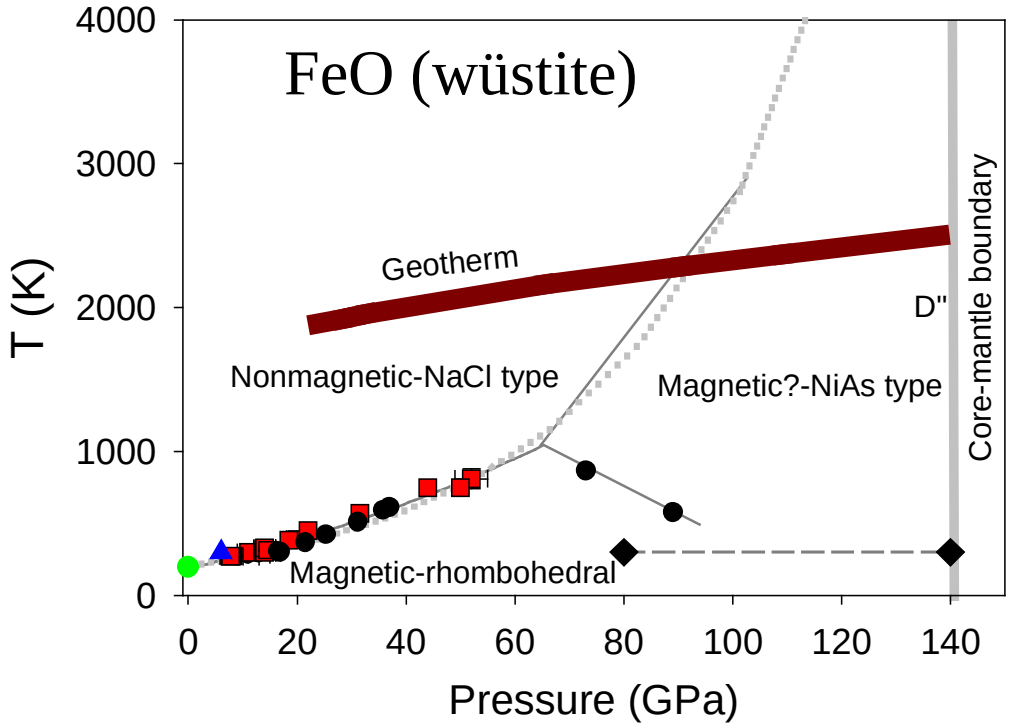

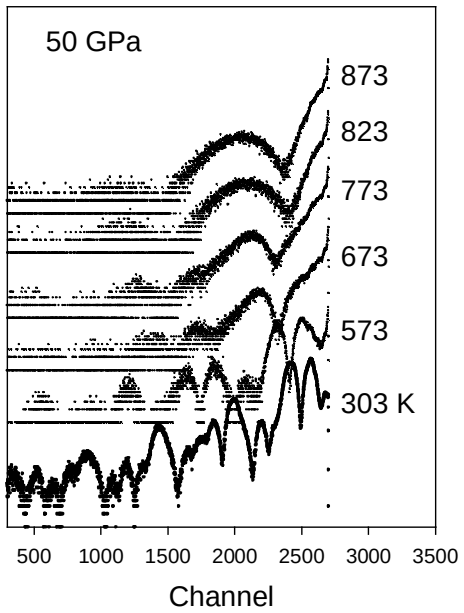

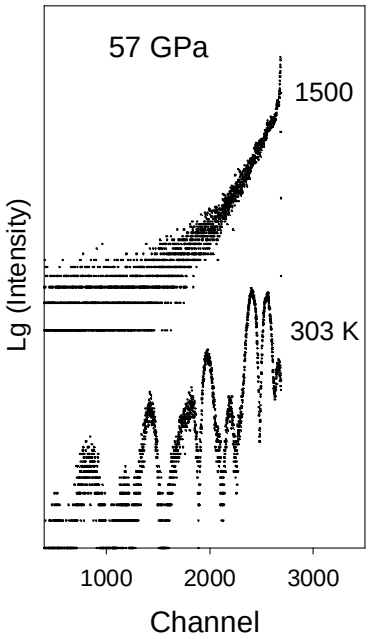

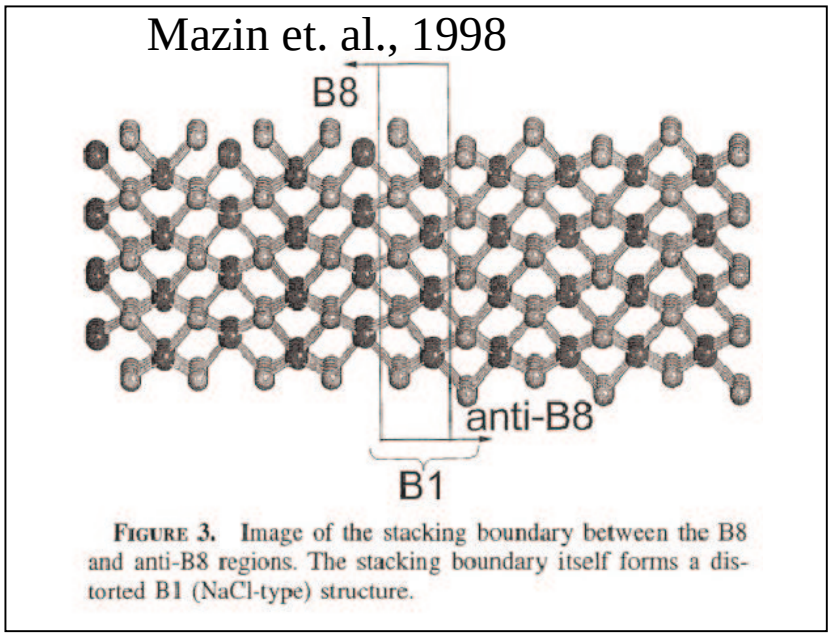

FIGURE 3. Image of the stacking boundary between the B8 and anti-B8 regions. The stacking boundary itself forms a distorted B1 (NaCl-type) structure.

Density of states (DOS) , compared with neutron data by Kugel (1977)

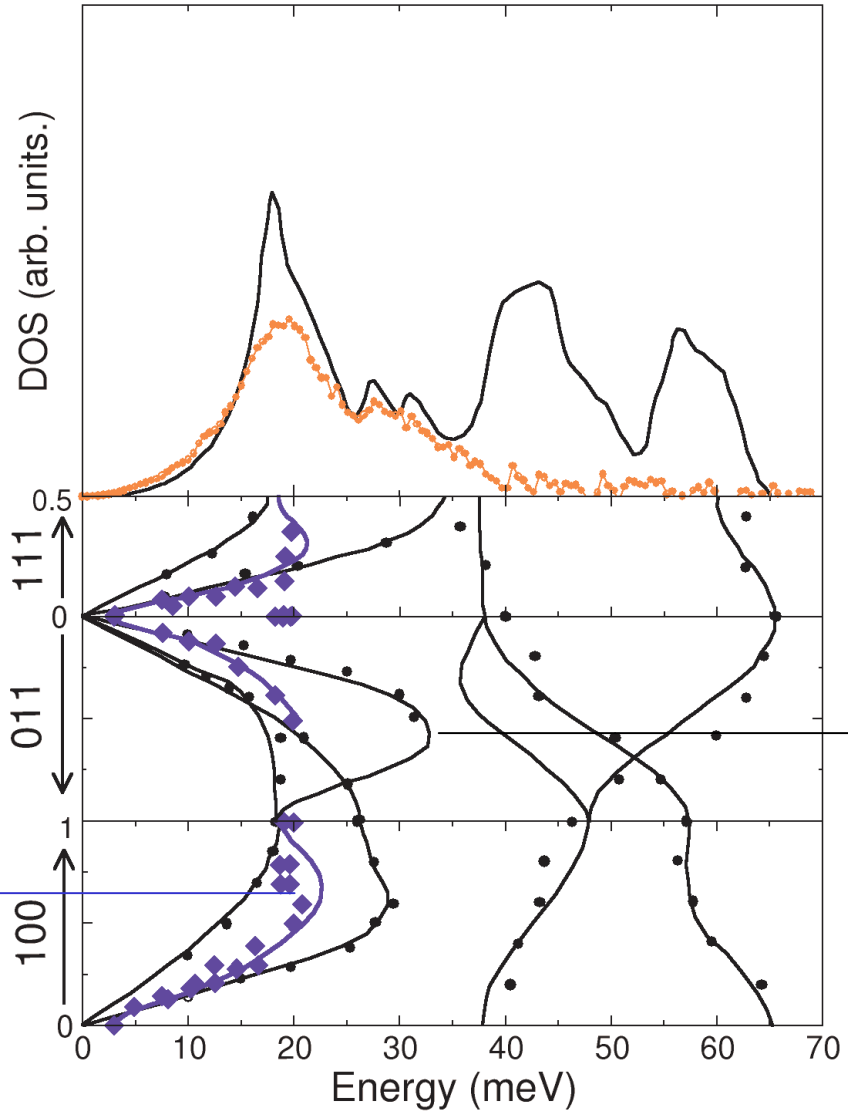

Phonons

Magnons

Debye-like part of DOS : $g(E)/E^2$

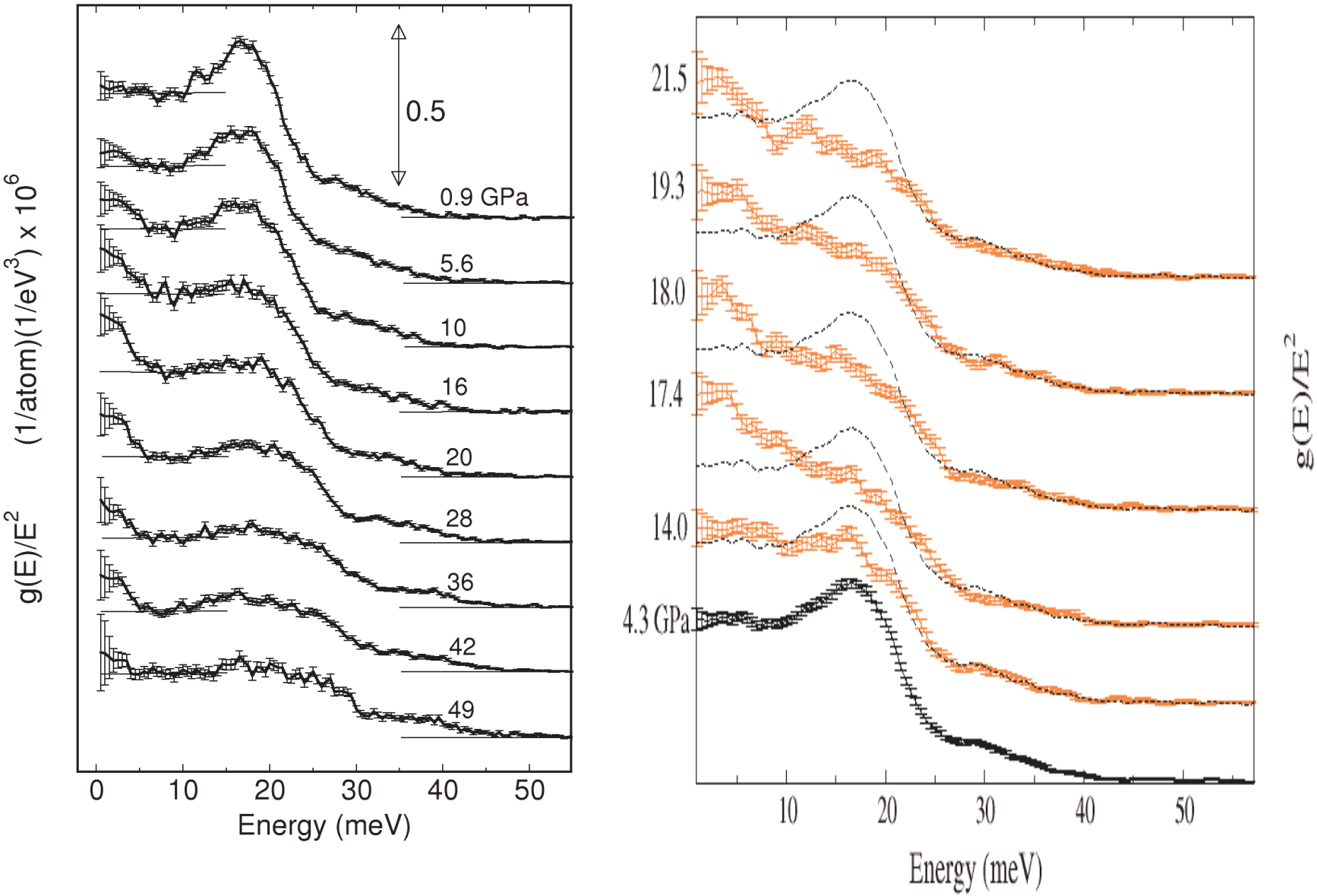

Magnetoelastic coupling (cubic crystal)

$$F = B_1(\alpha_1^2 e_{xx} + \alpha_2^2 e_{yy} + \alpha_3^2 e_{yy}) + B_2(\alpha_1 \alpha_2 e_{xy} + \alpha_2 \alpha_3 e_{yz} + \alpha_1 \alpha_3 e_{xz})$$ Magnetoelastic energy

$$+ (1/2)C_{11}(e_{xx}^2 + e_{yy}^2 + e_{zz}^2) + (1/2)C_{44}(e_{xy}^2 + e_{yz}^2 + e_{zx}^2)$$ Pure elastic contribution
$$+ C_{12}(e_{yy}e_{zz} + e_{xx}e_{zz} + e_{xx}e_{xx})$$

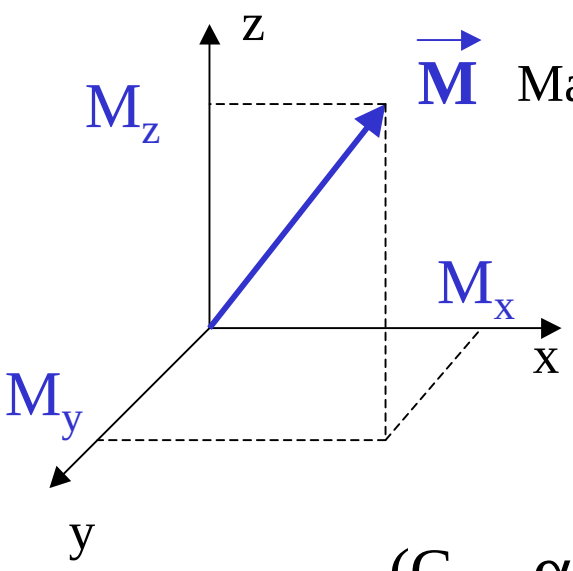

Magnetic moment, in antiferromagnet $\vec{\mathbf{M}} = \vec{\mathbf{M}}_1 - \vec{\mathbf{M}}_2 = 2\vec{\mathbf{M}}_1$

$$\alpha_1 = \frac{M_x}{|\mathbf{M}|} \qquad \alpha_2 = \frac{M_y}{|\mathbf{M}|} \qquad \alpha_3 = \frac{M_z}{|\mathbf{M}|}$$

Minimize F, and find (Kittel, 1949)

$$e_{ii} = \frac{(C_{12} - \alpha_i^2(C_{11}+2C_{12}))}{(C_{11}-C_{12})(C_{11}+2C_{12})} B_1 \,, \qquad e_{ij} = \frac{\alpha_i \alpha_j}{C_{44}} B_2$$

Magnetoelastic coupling
(Peletminskii, 1960)

From equations of motion of sound in antiferromagnet along magnetization axis (111):

$(\omega^2 - \omega_s^2)(\omega^2 - \omega_m^2) = M^2 B_2^2 k^2 g\Omega/2\rho$

ω_s - frequency of acoustic sound branch
$\omega_m^2 = \Omega g M(\beta + \alpha k^2)$ - magnetic dispersion branch
$\Omega = gM(\beta + 2\gamma)$
α , β, γ - exchange, and magnetic anisotropy
M - magnetic moment of the magnetic sublattice
B_2 - magnetoelastic coupling
ρ - density of the material
k - wavevector
g - gyromagnetic ratio
$B_2 = 2.5\ 10^{10}$ erg/cm^3, M=1400 Gauss,
$\alpha = 10^{-6}$ erg cm, $\rho = 6.2$ g/cm^2 , $\gamma = 0$
$\Omega = 2.6$ THz

Estimated coupling at 28 GPa

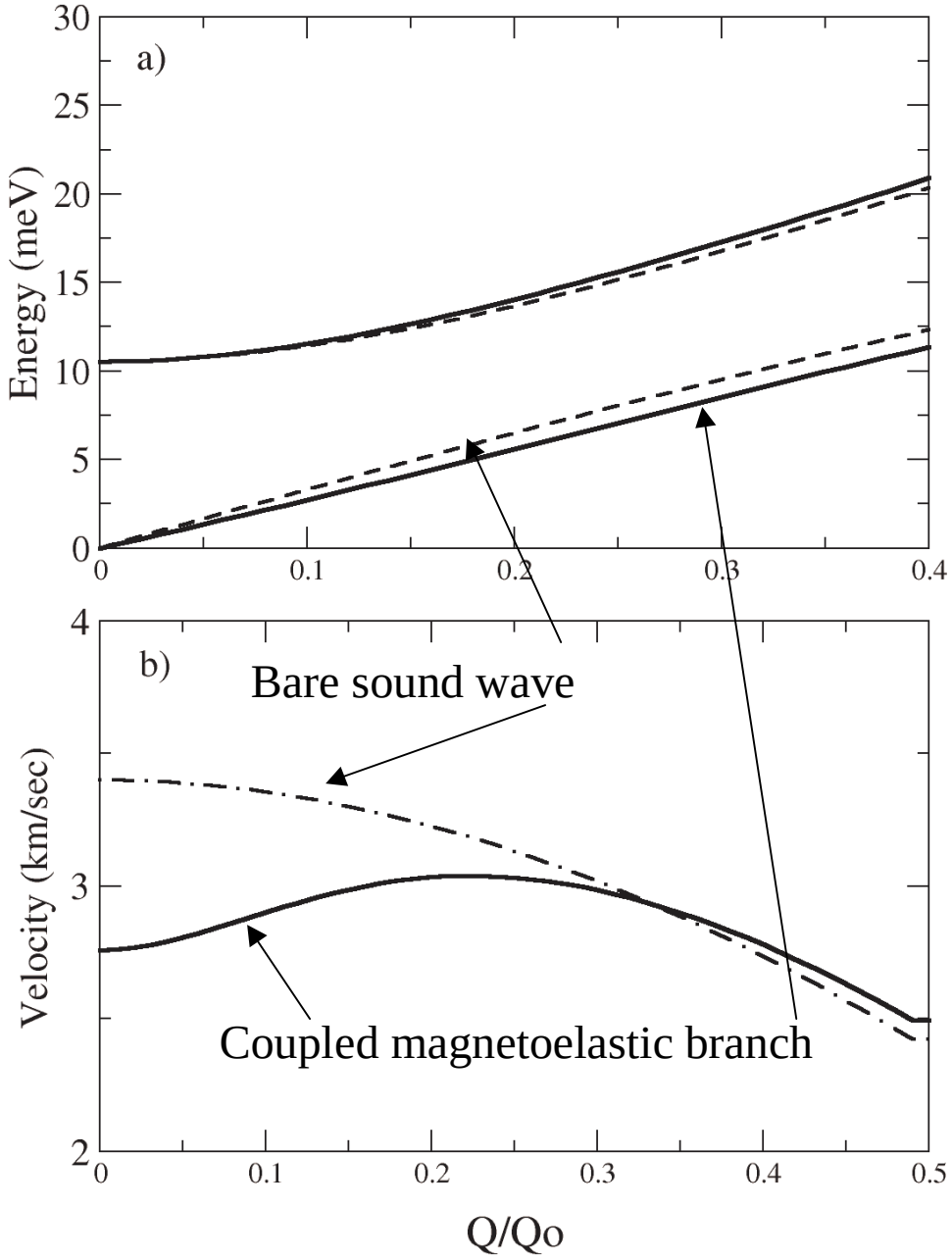

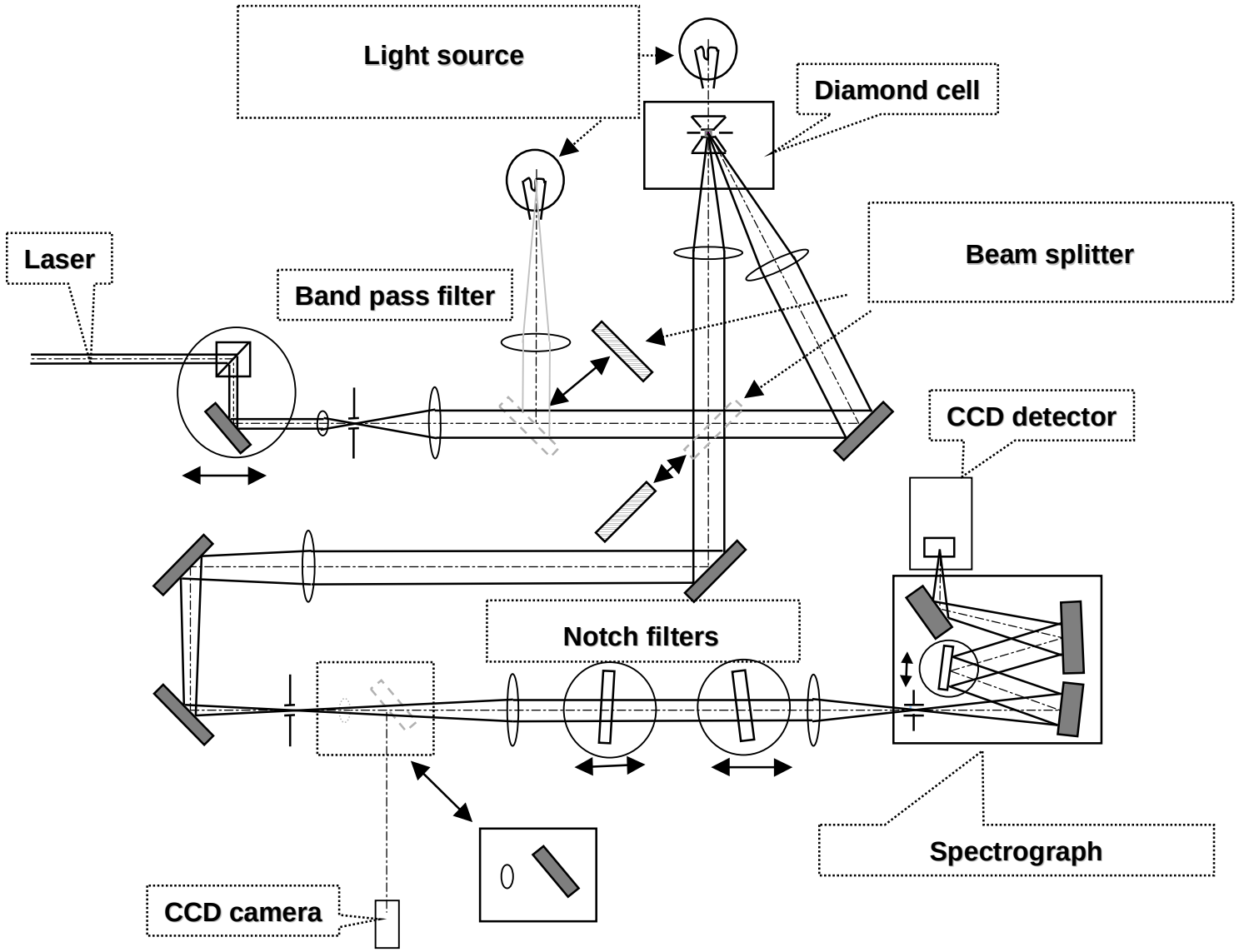

Raman setup

A. F. Goncharov, V. V. Struzhkin, JRS 2003

Magnetic excitations in FeO probed by Raman scattering

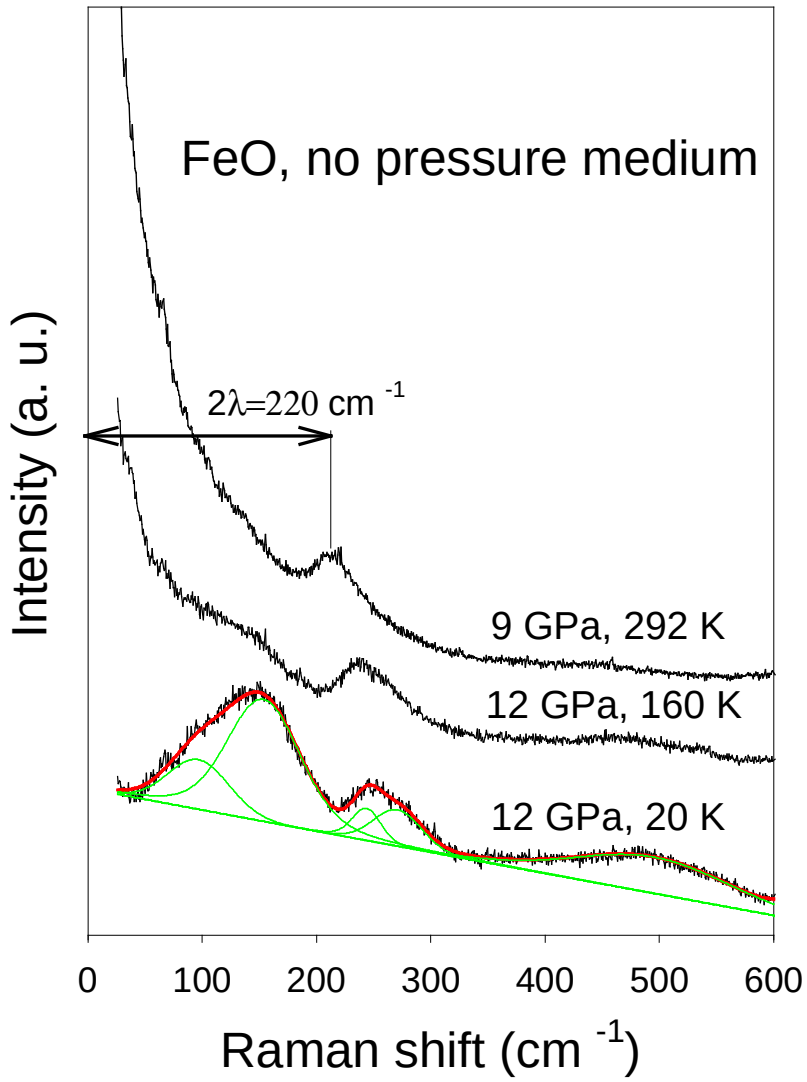

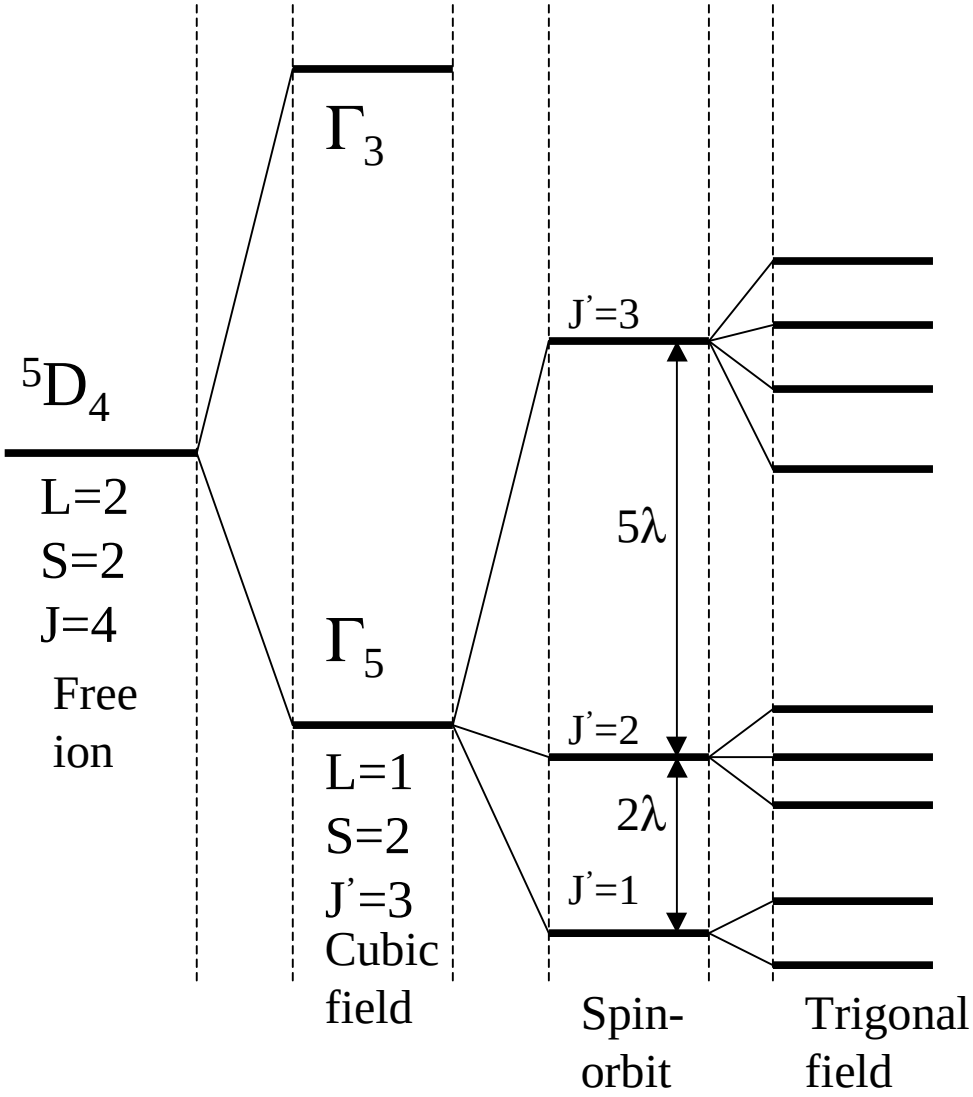

Magnetic excitations in FeO probed by Raman scattering

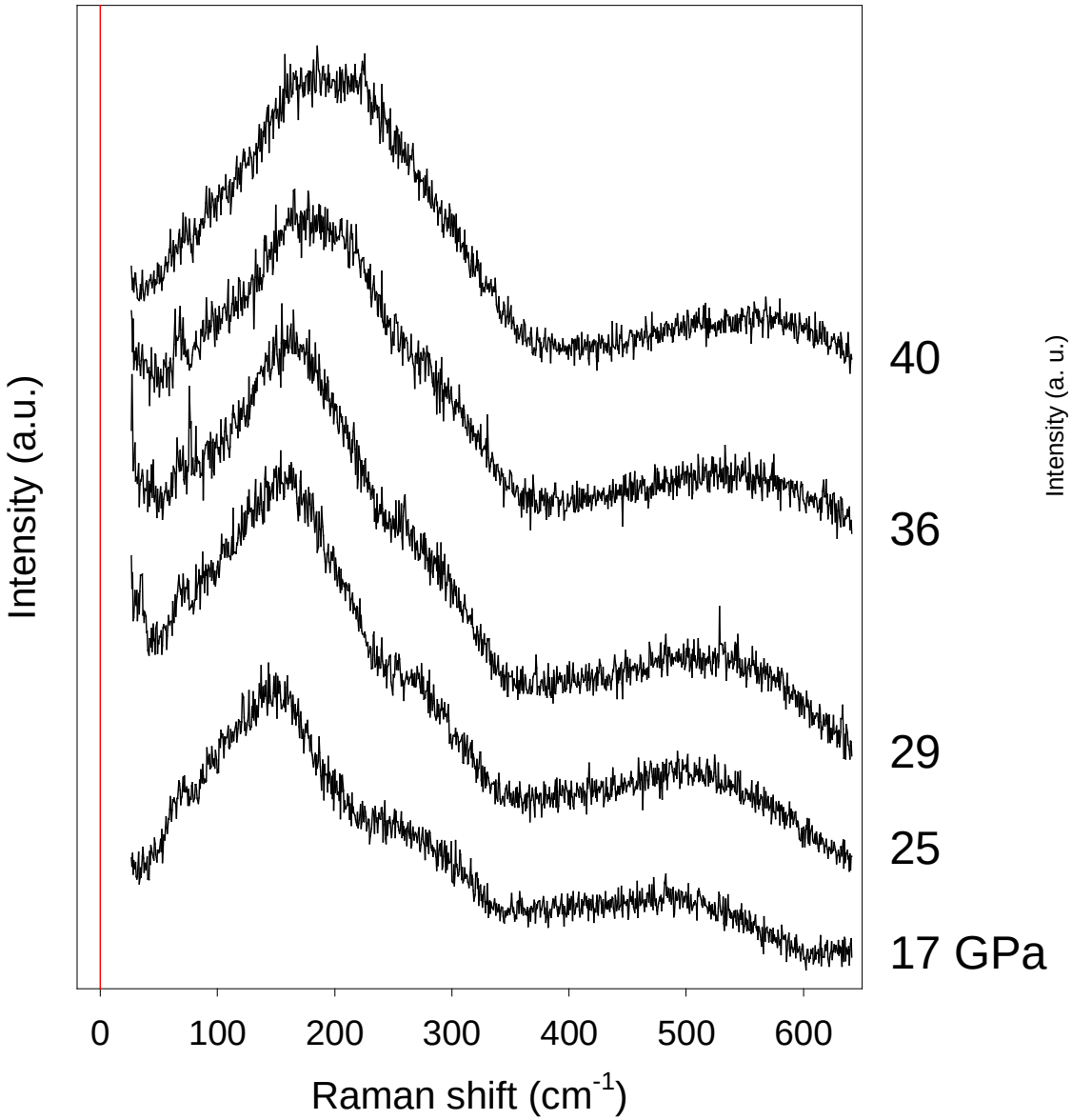

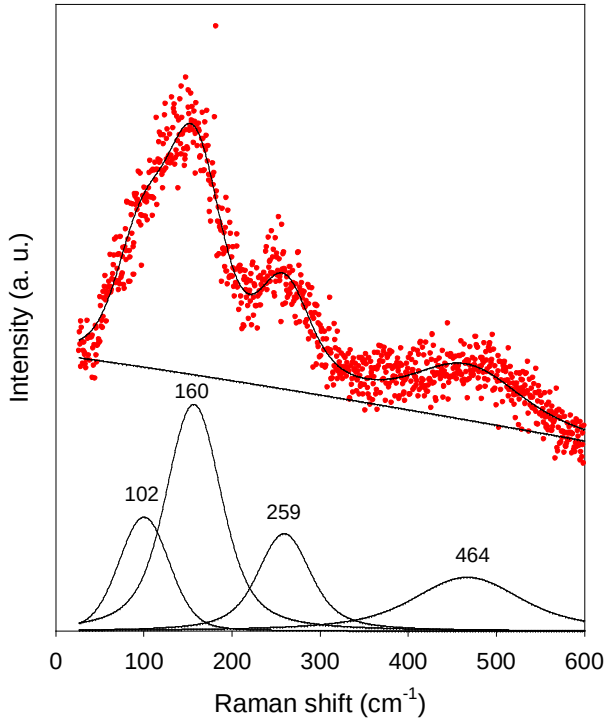

$$H = H_{ion} + H_{ex} = \sum_{\{jk\}} H_{so\text{-}cf}(jk) + \sum_{\{jk\}} \sum_{\{j'k'\}} J(jk,j'k')\, \boldsymbol{S}(jk)\, \boldsymbol{S}(j'k').$$

$$H = H_i + H'_{ex} = (H_{ion} + H_{mf}) + (H_{ex} - H_{mf}),$$

$$H_{mf} = \sum_{\{jk\}} (-1)^k H_z S_z(jk), \quad H_z = 2\sum_{\{r\}} Z_r J_r \langle S_z \rangle$$

$$H_i = \sum_{\{jk\}} [\, H_{so\text{-}cf}(jk) + (-1)^k H_z S_z(jk)] = \sum_{\{jk\}} H_{jk}$$

$$H_{so\text{-}cf} = -\alpha\lambda(\boldsymbol{LS}) + C_z L_z^2 + D_z S_z^2 + C_{xy}(L_x^2 - L_y^2) + D_{xy}(S_x^2 - S_y^2)$$

$$a(kp,\boldsymbol{q}) = N^{-1/2} \sum_{\{j\}} a_p(jk) \exp\{i\, \boldsymbol{q}\, \boldsymbol{R}(jk)\}$$

L=1

S=2

J_{1+}=1.8 cm^{-1}

J_{1-}=1 cm^{-1}

Magnetic excitations in FeO probed by Raman scattering:

model Hamiltonian with spin-wave excitations

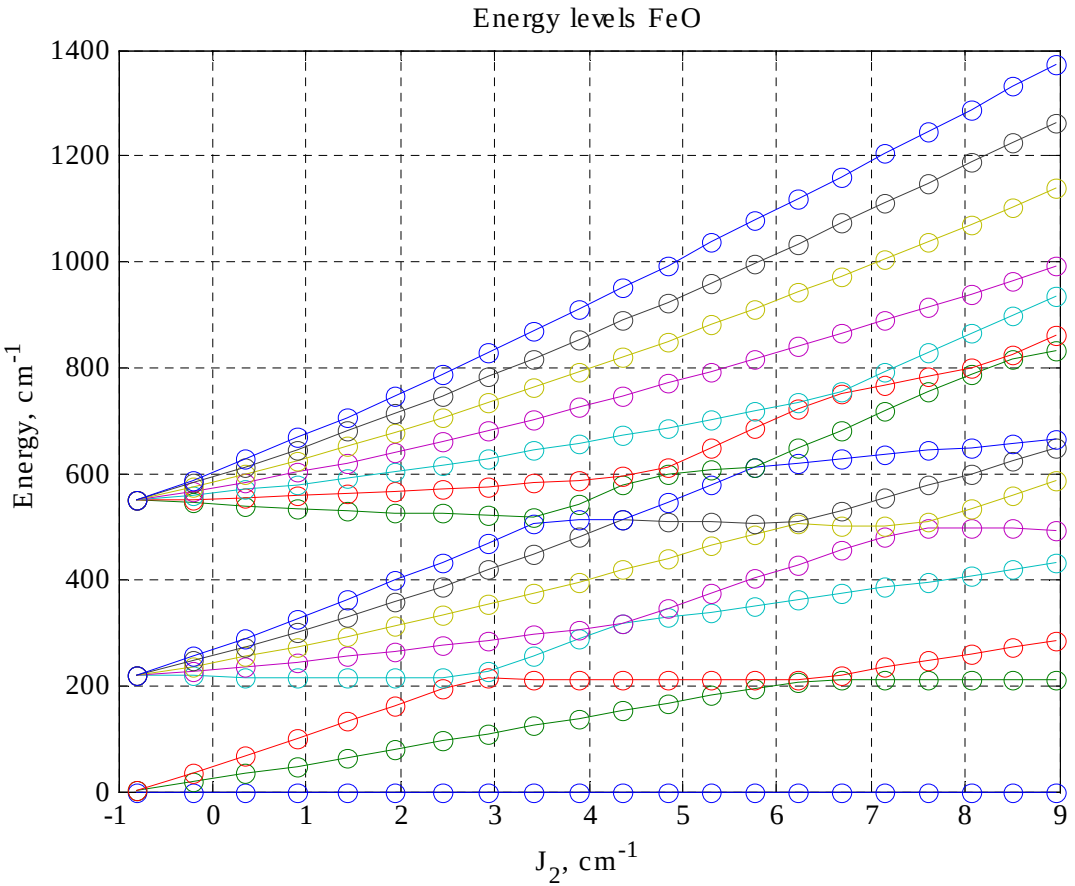

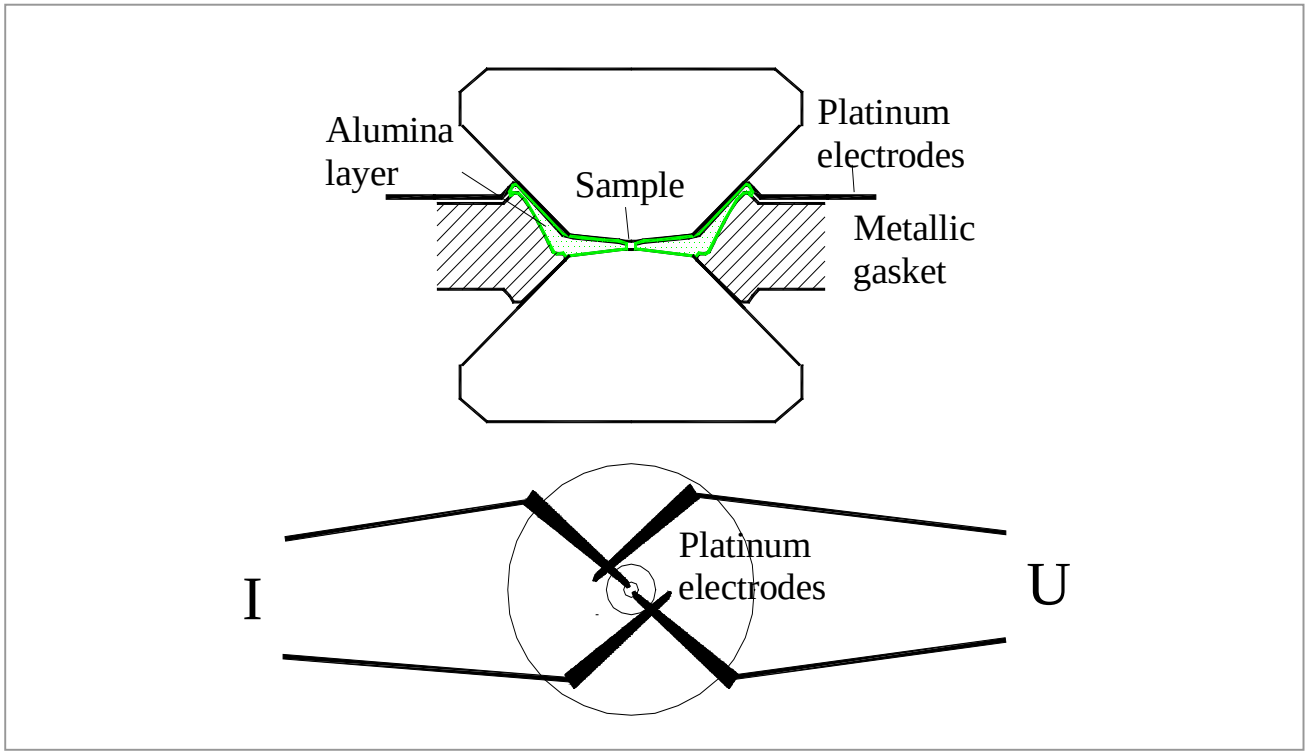

Electrodes

- Foils and wires
- Sputtering techniques

Insulating layer

- Epoxy mixed with cubic BN, diamond or other powders
- Compacted Al_2O_3 powder
- CVD diamond coating

M. I. Eremets, V. Struzhkin, 2004

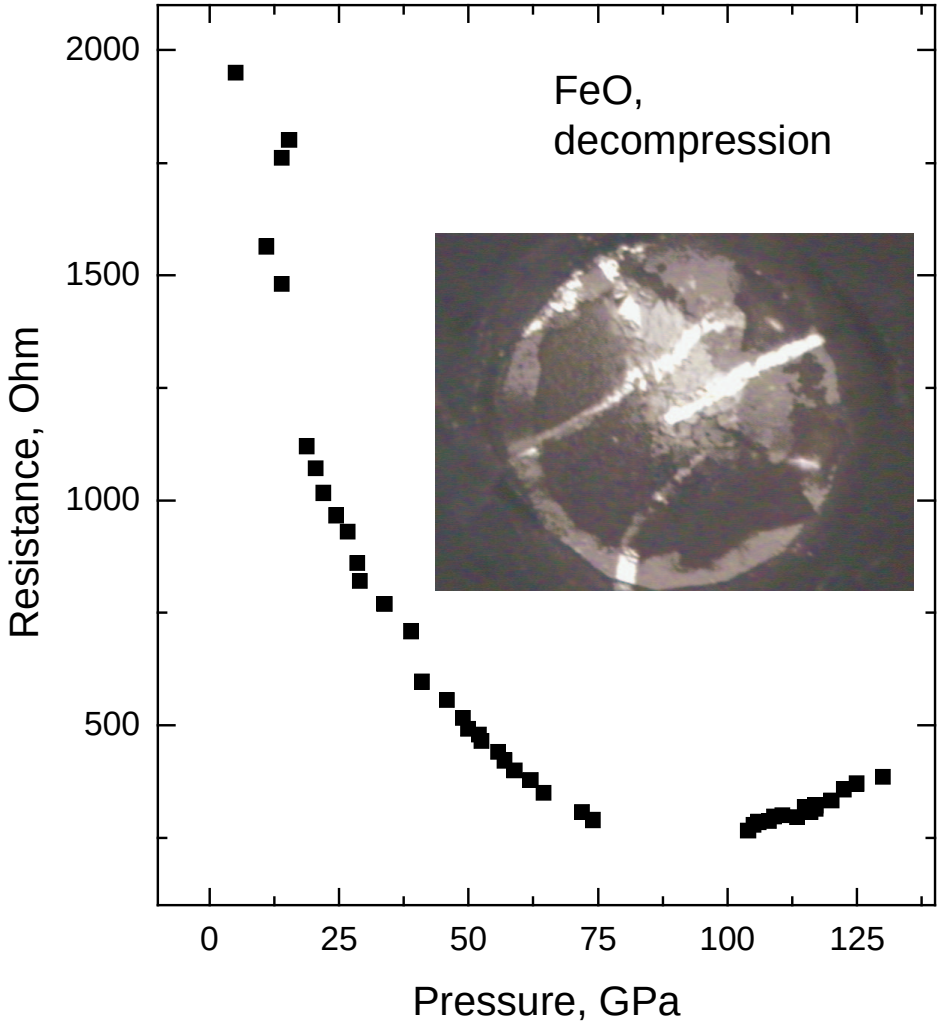

S. T. Weir, et. al. 1999, AIRAPT-17

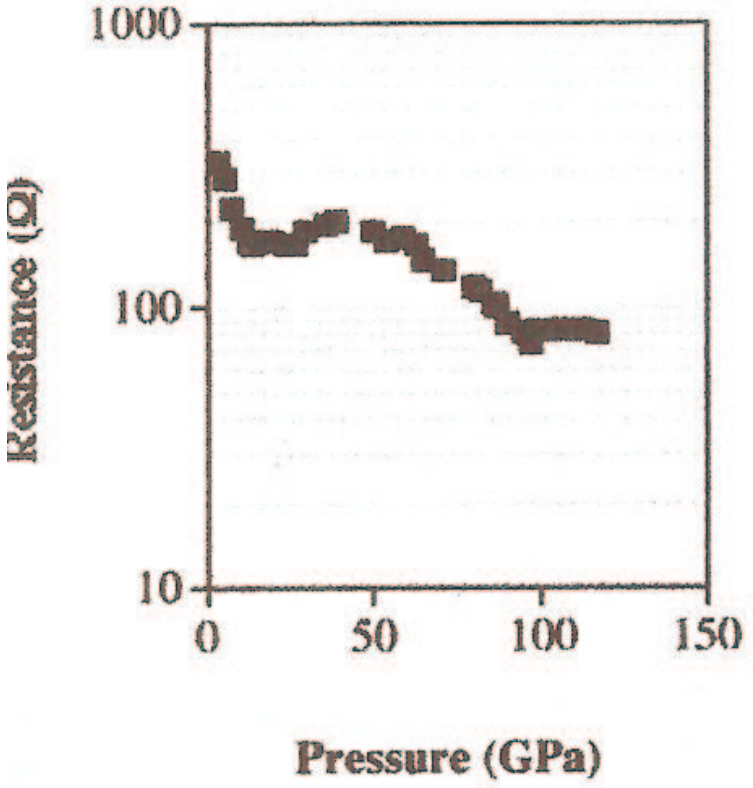

Conclusions: FeO

• Magnetic phase diagram below 60 GPa is in very good agreement with x-ray diffraction data

• Magnetic properties of the high-pressure modification : the spin state of Fe^{2+} in a “metallic” FeO at pressures above 100 GPa is still an open question

• Inelastic scattering reveals a strong magnetoelastic coupling

• Resistance measurements are compatible with a sluggish transition to a “nearly” metallic state in the range from 70 to 140 Gpa (conductivity ~ 1 Ω^{-1} cm^{-1})

NRIXS of Fe in He pressure medium

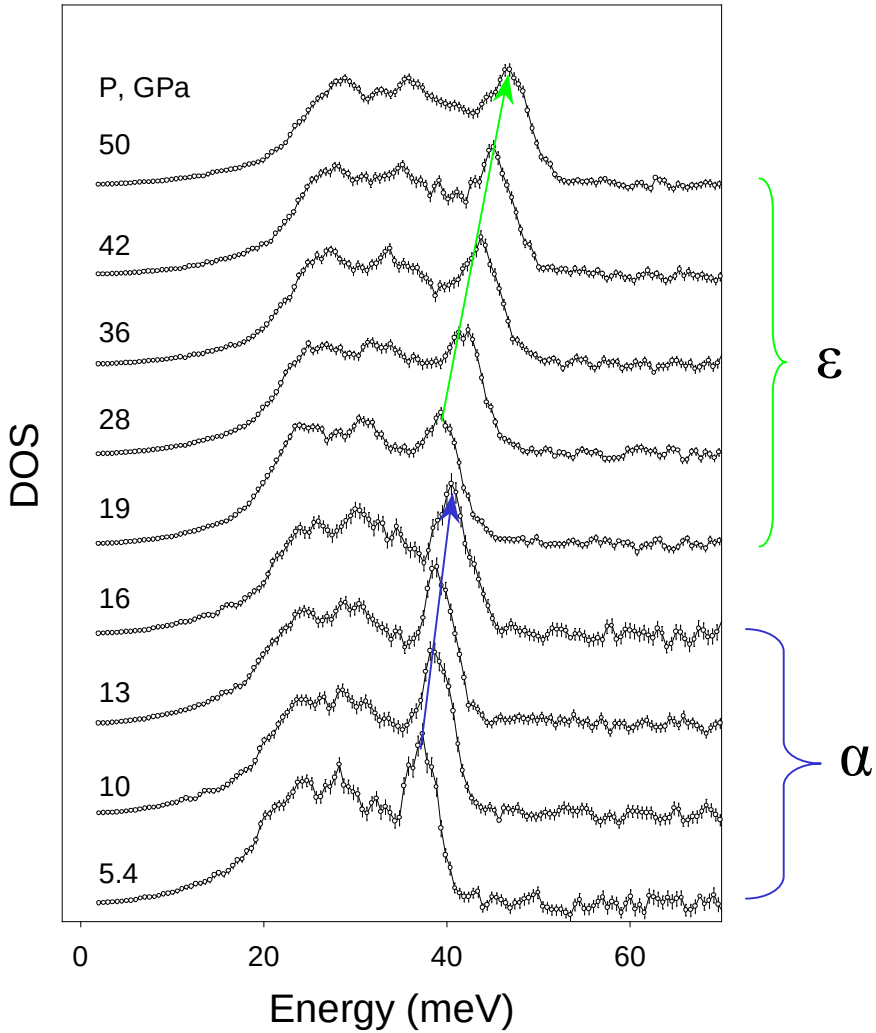

Theory,
L. Vocadlo et al.

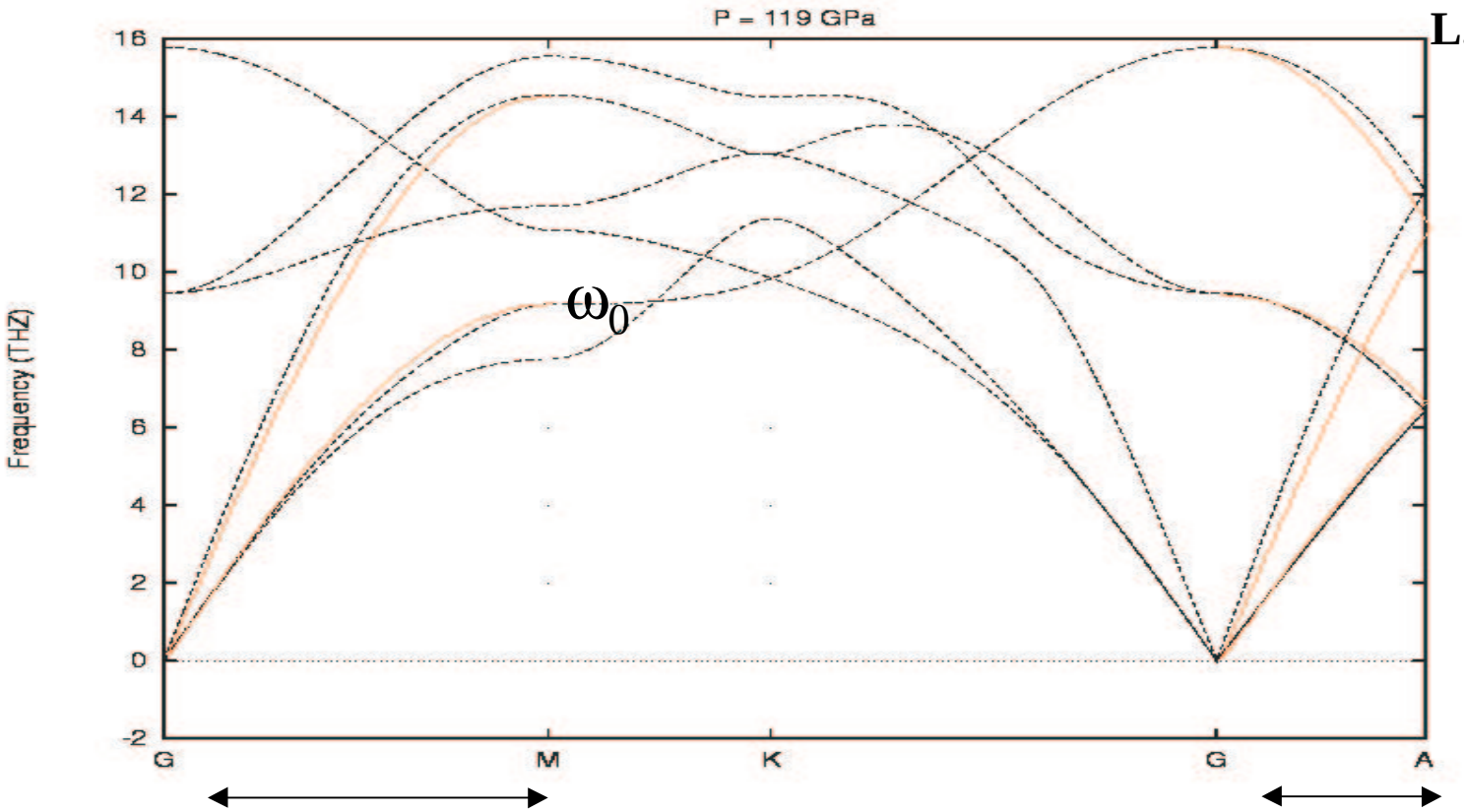

$Q_0 = g_2 = 2\pi/a\sqrt{3}$

$V = (\pi/2)\,\omega_0 / Q_o$

$C_k = \rho V^2$

$Q_o = 2g_3 = 4\pi / c$

Antonangeli et. Al., EPSL 2004

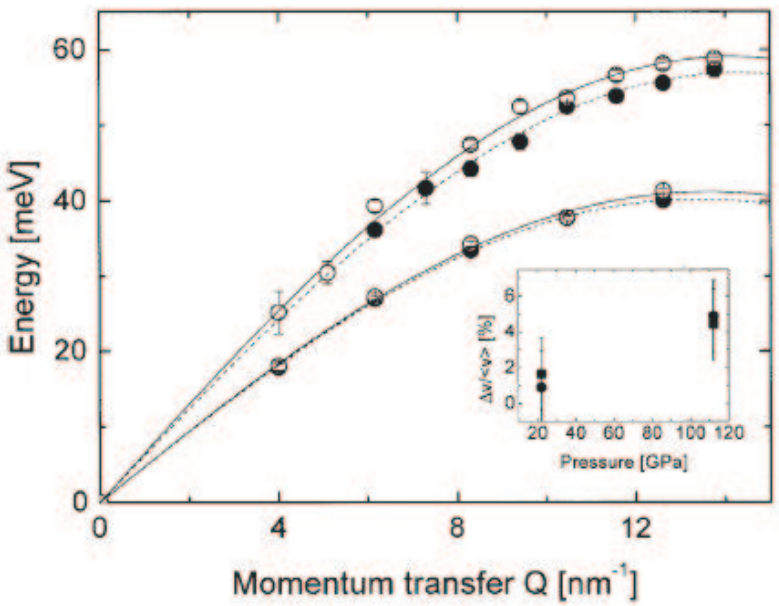

Fig. 4. LA phonon dispersion curves of iron at room temperature and at pressures P of 22 GPa (lower curve) and 112 GPa (upper curve) for the two orientations of the DAC; full (open) circles: sound propagation at 90° (50°) to the DAC loading axis. The displayed error bars of the energy position results from the statistic error of the fit and the finite Q-resolution of the spectrometer. The lines through the data points are fits to the data, with Q_{max} as a free parameter. The inset reports the relative difference of the sound speeds $\Delta v/\langle v\rangle$ as a function of pressure. The two methods used to derive the sound speed (see Section 3.1) yield slightly different results, indicated by full circles (Q_{max} free) and squares (Q_{max} fixed).

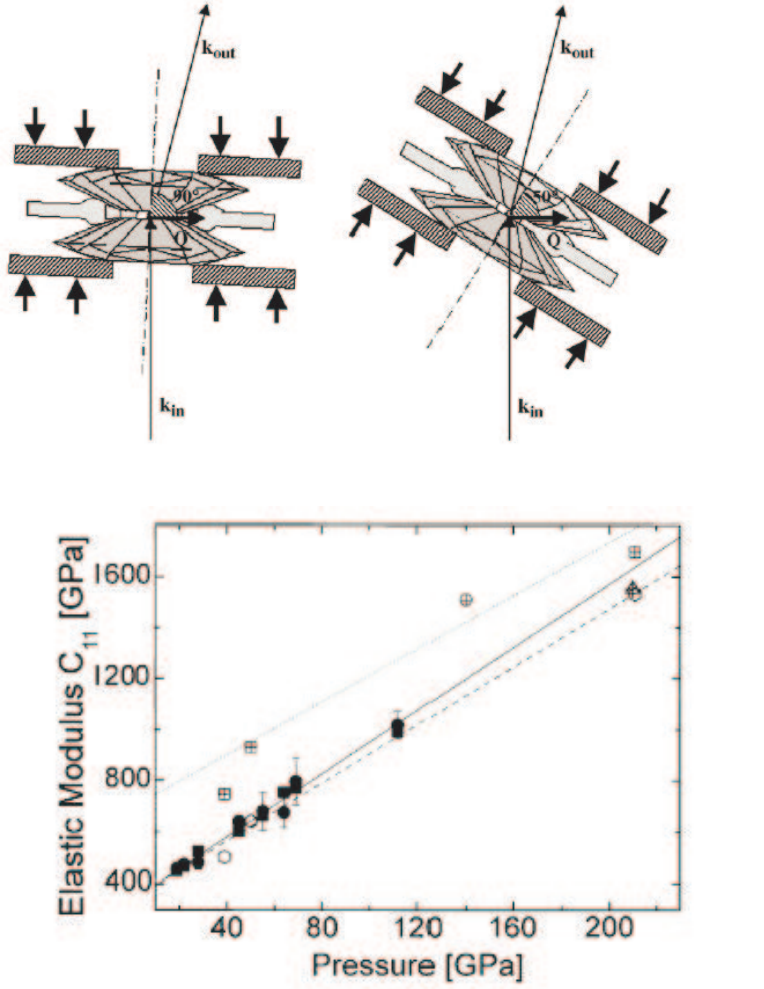

Fig. 6. Derived elastic modulus C_{11} as a function of pressure. Full circles (squares): IXS data analysed with Q_{max} free (fix), solid (dashed) line: corresponding linear fits to the IXS data with Q_{max} free (fix); hexagons: XRD data [18,27]. All the experimental results are at room temperature. Calculations at 0 K: crossed squares [21,23], crossed circles [20], and dotted line [22]. Calculations at 300 K: crossed triangles [24].

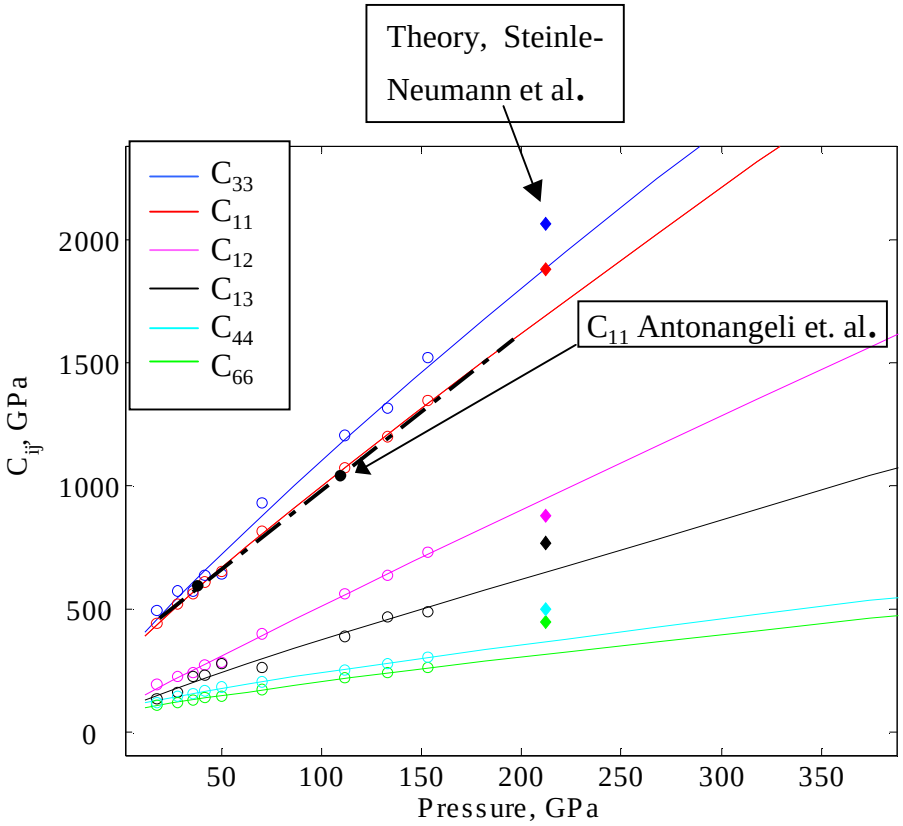

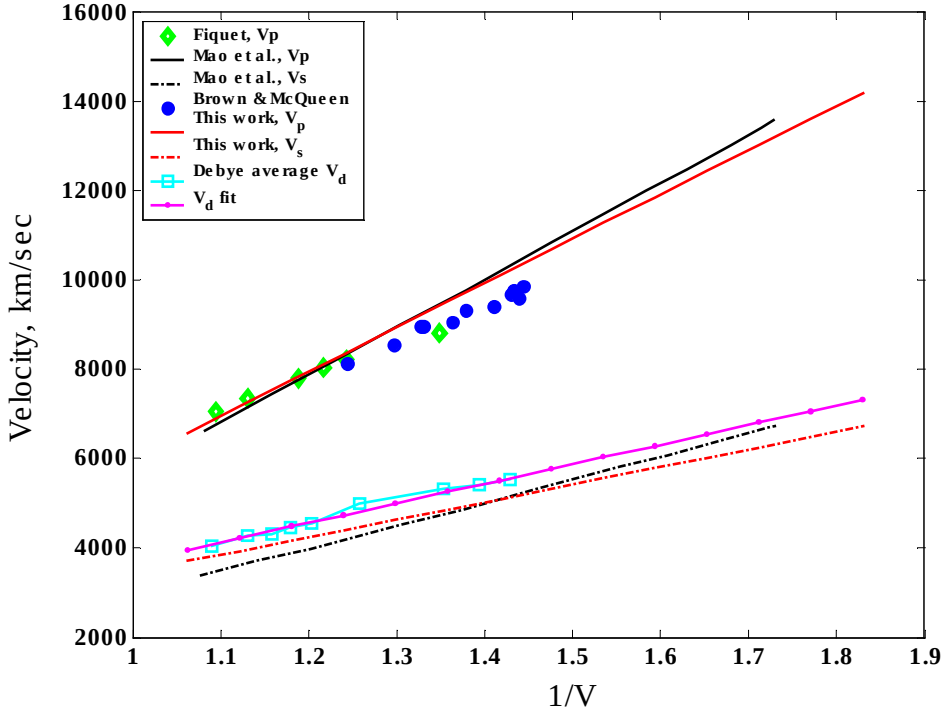

	C_{44}	C_{33}	C_{11}
Theory	0.91	1.15-1.05	1.10

Best fit with theoretical shape for dispersion branches, using bulk modulus, and Debye average velocity V_d as constraints.

Kohn, Chumakov, Rüffer, 1998

Nuclear resonant inelastic absorption of synchrotron radiation in an anisotropic single crystal

$FeBO_3$

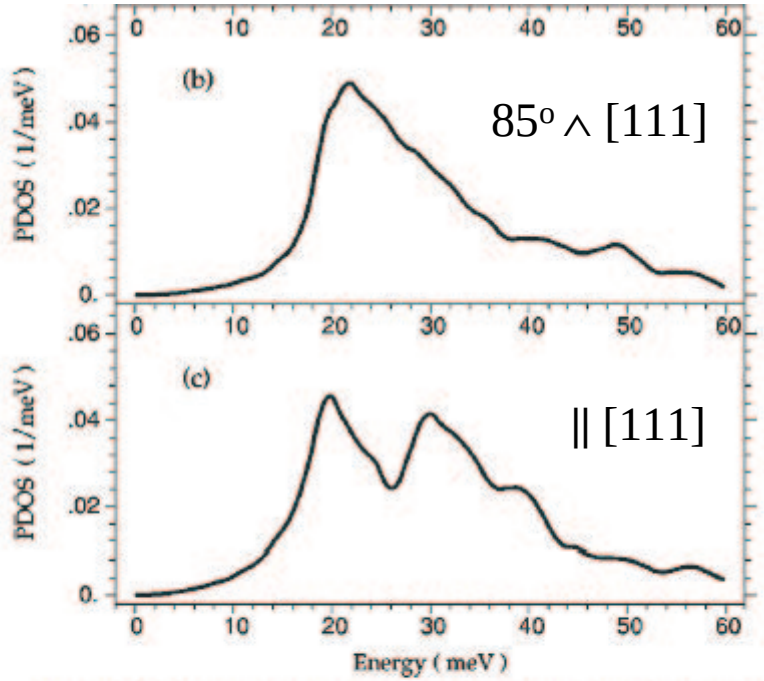

FIG. 2. Results of processing the experimental data from Fig. 1. (a) DOS for the polycrystalline α-iron foil, (b),(c) PDOS for the $^{57}FeBO_3$ single crystal in the cases where the axis of projection has the angle of (b) 85° relative to the [111] axes, or (c) parallel to the [111] axes.

$$g_m(E,\mathbf{s}) = V_0 \sum_j \int \frac{d\mathbf{q}}{(2\pi)^3} \delta[E - \hbar\omega_j(\mathbf{q})] |\mathbf{s}\cdot\mathbf{e}_{mj}(\mathbf{q})|^2$$

$$= \frac{V_0}{(2\pi)^3} \sum_j \int \frac{dq_1 dq_2}{|\mathrm{grad}_{\mathbf{q}} \hbar\omega_j(\mathbf{q})|} |\mathbf{s}\cdot\mathbf{e}_{mj}(\mathbf{q})|^2.$$

s=**k**/k,

$\mathbf{e}_{mj}$ - polarization of the phonon

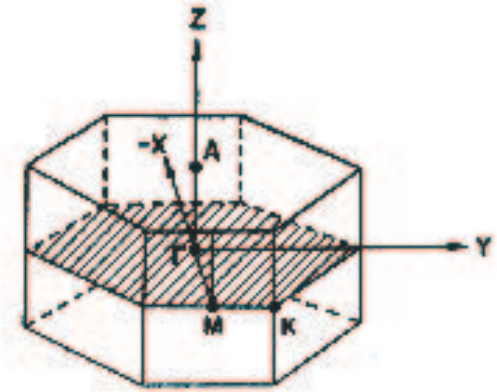

Wenk et al., Nature (2000)
ε-Fe at 220 GPa

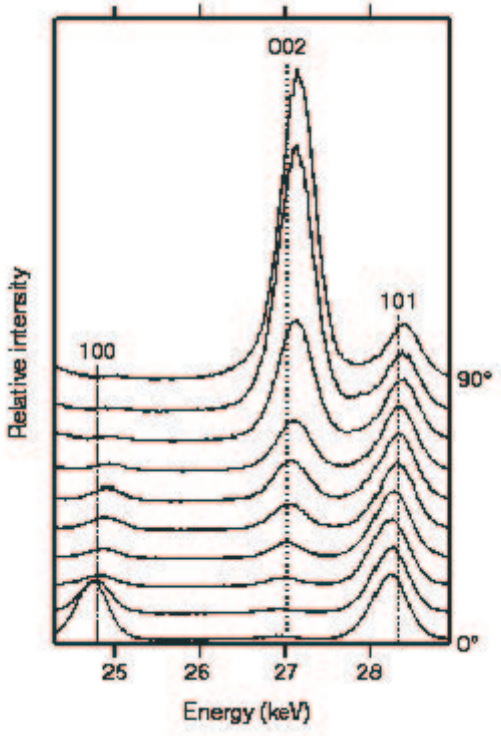

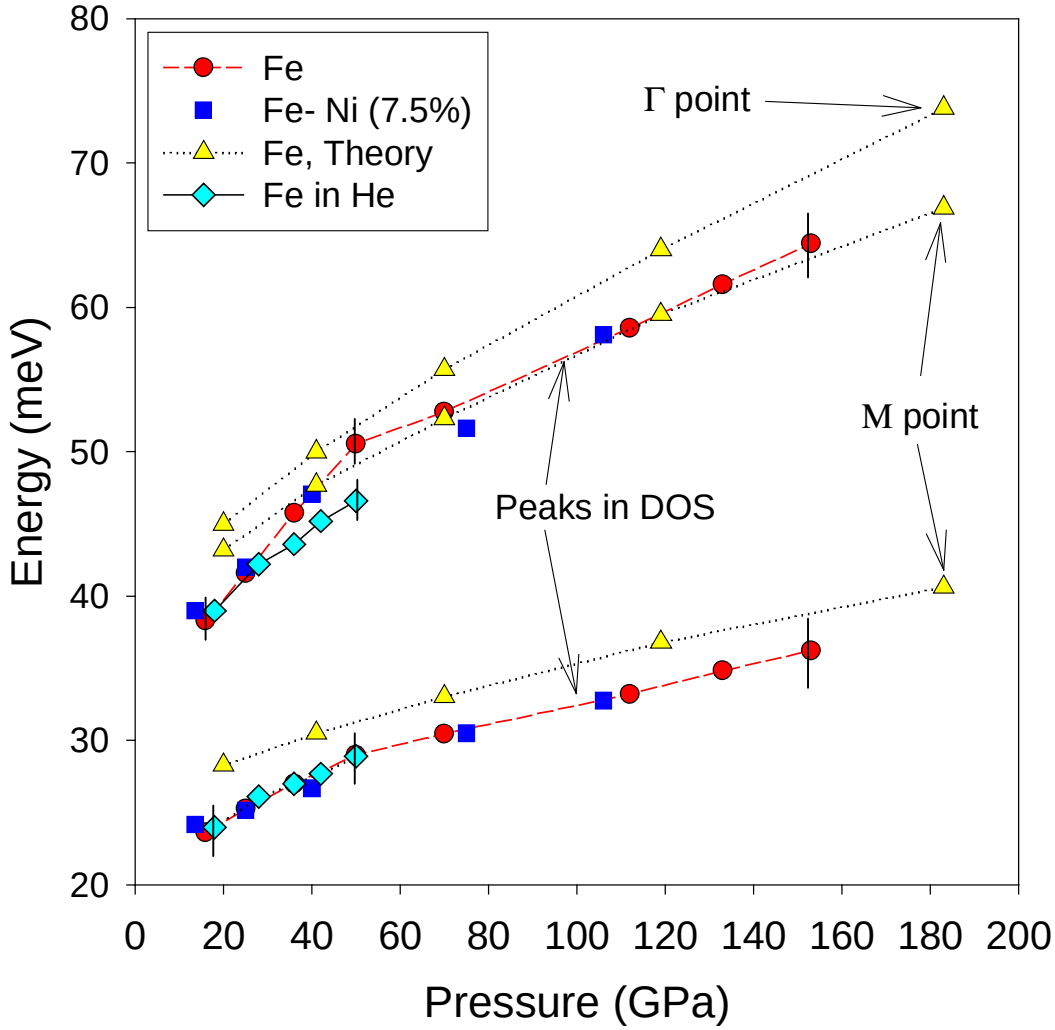

Empirical correction
ΔP=15 GPa
brings theory into better agreement with experiment, assuming that the sample has strong preferred orientation above 50 GPa

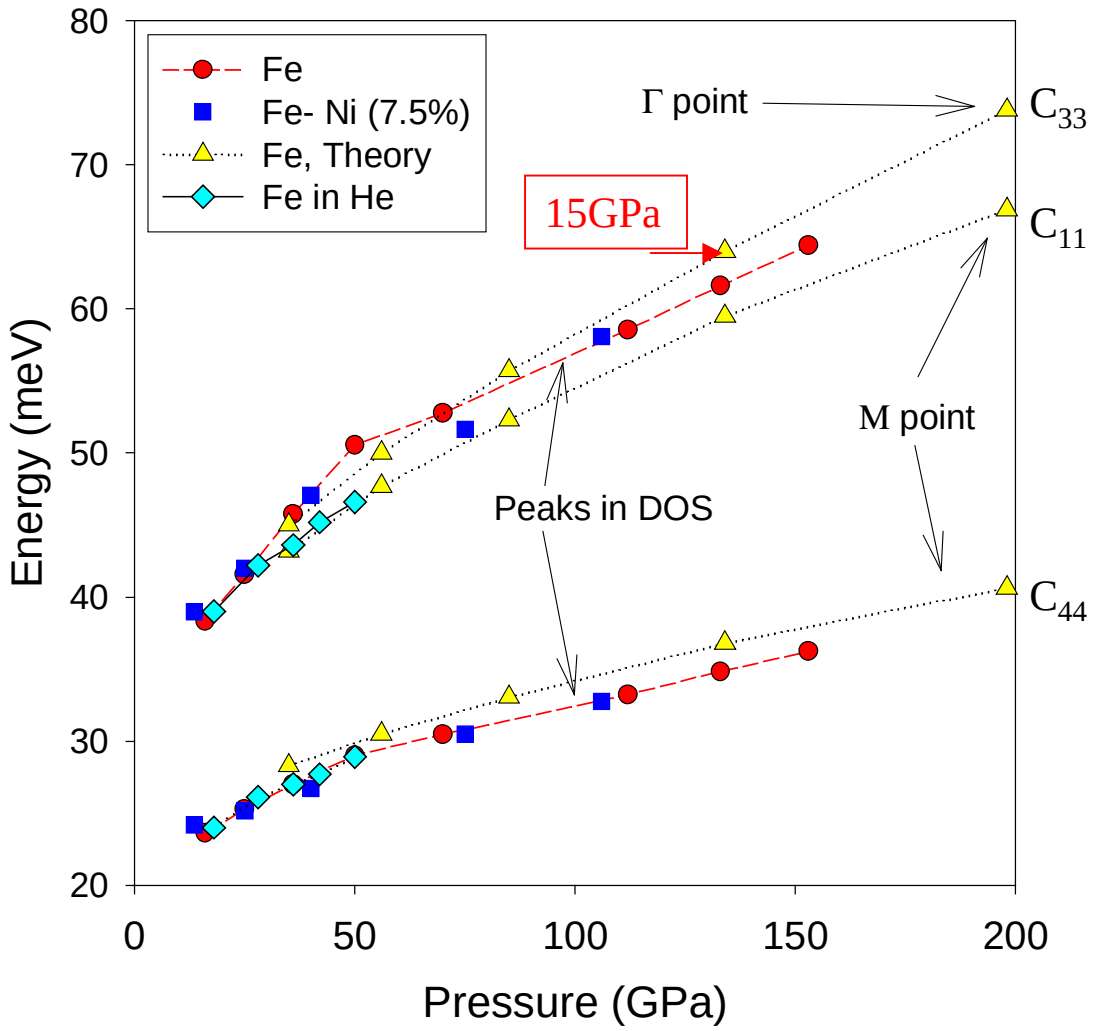

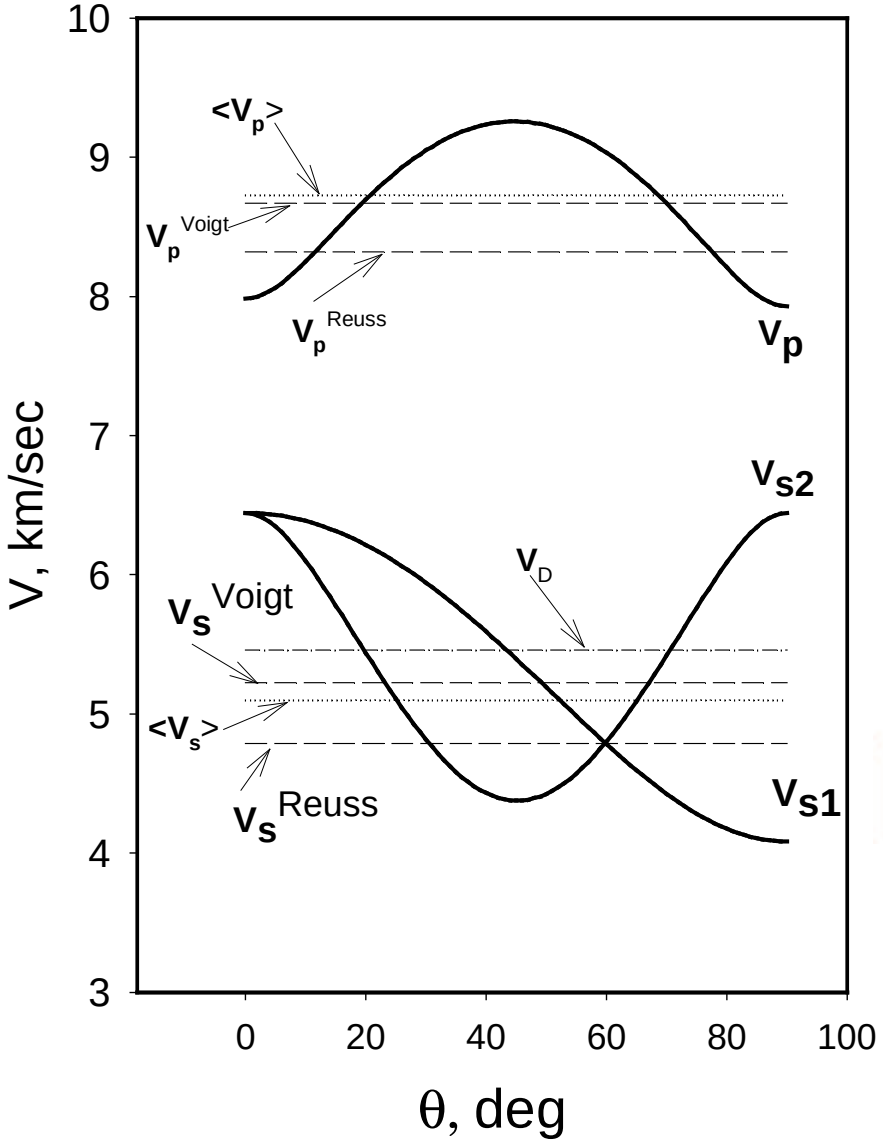

$$3V_D^{-3} = V_P^{-3} + 2V_S^{-3}$$

$$2V_S^{-3} = V_{S1}^{-3} + V_{S2}^{-3}$$

$$\rho V_p^2 = \frac{(A+B)}{2}$$

$$\rho V_{s1}^2 = C_{44} + \frac{1}{2}(C_{11} - C_{12} - 2C_{44})sin^2\theta$$

$$\rho V_{s2}^2 = \frac{(A-B)}{2}$$

$$A = C_{11} + C_{44} + (C_{33} - C_{11})cos^2\theta$$

$$B = \frac{1}{2}\{(C_{11} - C_{33})^2 + 4(C_{13} + C_{44})^2 - 2(C_{11} - C_{33})(C_{11} + C_{33} - 2C_{44})cos2\theta + \left[(C_{11} + C_{33} - 2C_{44})^2 - 4(C_{13} + C_{44})^2\right] cos^2 2\theta\}^{\frac{1}{2}}$$

V_p - compressional wave
V_{S1}- pure shear wave
V_{S2} - quasi shear wave

Anharmonicity of shear wave in Fe: Raman results (Goncharov, Struzhkin, in JRS, 2003)

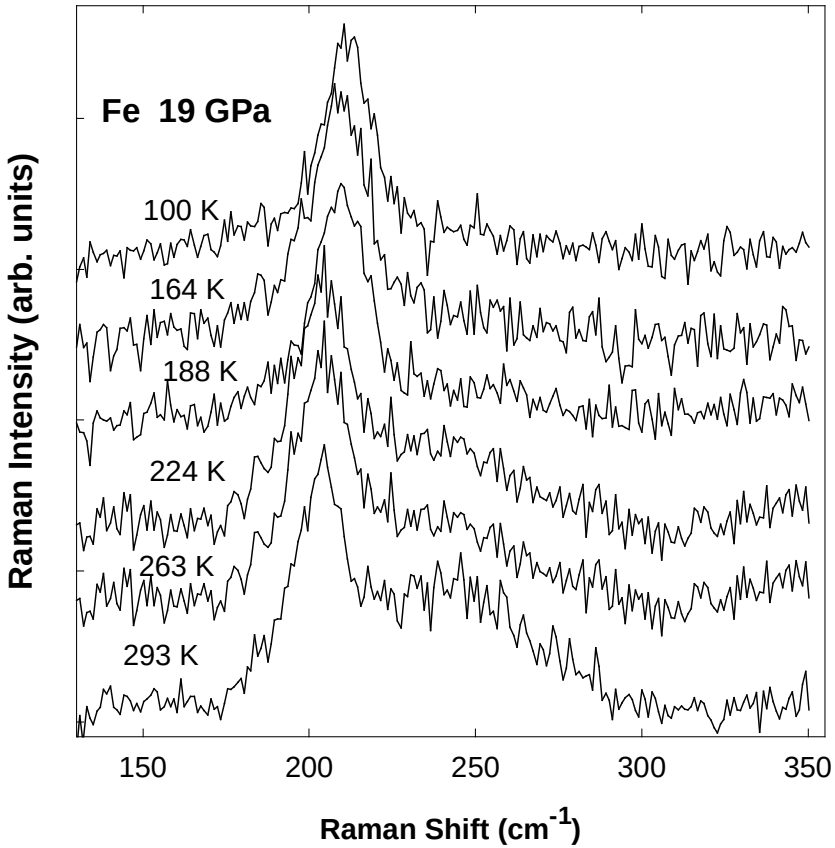

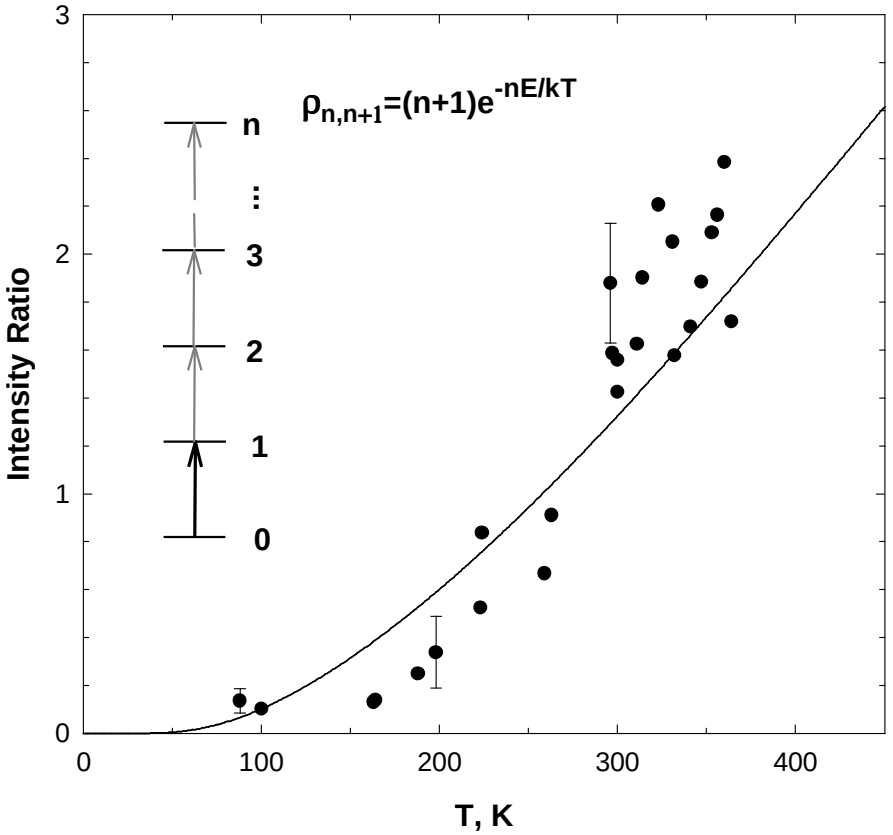

Anharmonicity of shear wave in Fe: Raman results

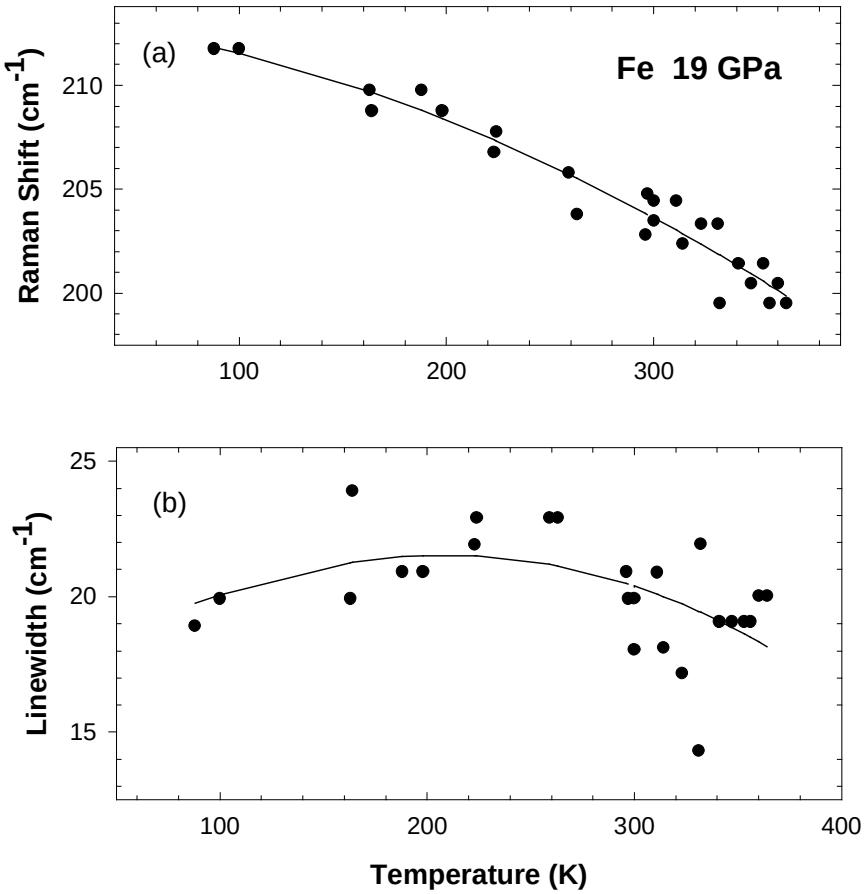

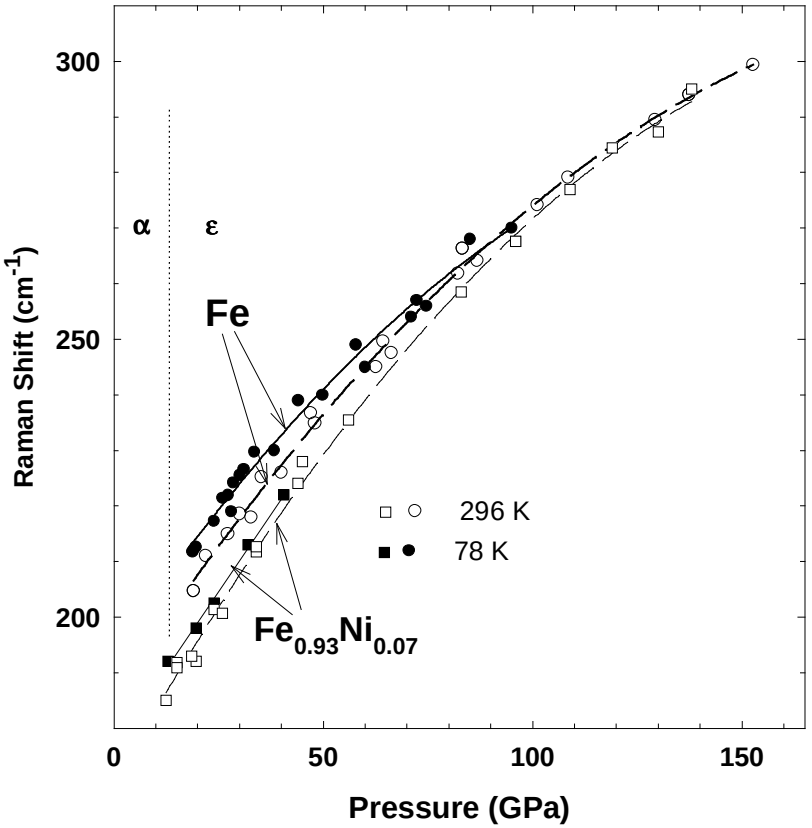

Conclusions: Fe, Fe-Ni

- Van-Hove singularities: dispersion branches in high symmetry directions may be used to estimate C_{ij}.

- Hydrostatic versus non-hydrostatic measurements (using preferred orientation) may provide additional C_{ij}.

- Fe-Ni(7%) alloy has shear-wave elastic properties very similar to pure Fe: with present data accuracy it is not possible to specify the content of Ni in the Earth's core.